WILEY

Carbon Neutralization

REVIEW OPEN ACCESS

Optimization Strategies and Mechanisms of High-Concentration Electrolytes for Aqueous Rechargeable Batteries

Lingli Chen[1] | Yue Xu[1,2,3] | Angran Liu[1] | Bo Cheng[1] | Sihan Wang[1] | Xiaolin Zhang[3] | Yongbin Hua[1] | Long Jiang[1] | Chun Fang[2] | Jiantao Han[2] | Paul K. Chu[3]

[1]School of Physics and Optoelectronic Engineering, Yangtze University, Jingzhou, China | [2]State Key Laboratory for Materials Processing and Die & Mould Technology, School of Materials Science and Engineering, Huazhong University of Science and Technology, Wuhan, China | [3]Department of Physics, City University of Hong Kong, Hong Kong, China

Correspondence: Yue Xu (yuexu@yangtzeu.edu.cn) | Chun Fang (fangchun@hust.edu.cn)

Received: 12 May 2025 | **Revised:** 22 June 2025 | **Accepted:** 11 July 2025

Funding: This work was supported by the National Natural Science Foundation of China (Nos. 22479057, 51902118), International Postdoctoral Exchange Fellowship Program (Grant No. PC2021026), Postdoctor Project of Hubei Province under Grant Number 2024HBBHXF083, and City University of Hong Kong Donation Research Grants (No. DON-RMG 9229021 and No. 9229021).

Keywords: aqueous electrolyte | electrochemical windows | electrolyte modifications | hydrogen-bond network | solvation structure

ABSTRACT

Aqueous batteries represent a significant research area due to their low cost and high safety advantages. However, aqueous electrolytes suffer from high side-reaction activity, narrow electrochemical windows, and insufficient interface stability and are frozen at low temperatures, thus hampering practical applications. This review focuses on high-concentration brine-based aqueous electrolyte optimization strategies to address the above problems. The solvation structure, hydrogen-bond network, and interfacial components are the key factors that are altered by the appropriate salts, solvent selection, and electrode interaction. A high concentration of brine decreases the free water content, inhibits the hydrogen evolution reaction (HER) and oxygen evolution reaction (OER), and widens the electrochemical window. Additional salts and solvents in the electrolyte can further promote the formation of the solid electrolyte interphase (SEI) and the cathode electrolyte interphase (CEI) to reduce deleterious interfacial side reactions. At the same time, the synergistic effects between the cathodes/anodes and the electrolyte expand the electrochemical window, improve the interface stability, and enhance the electrochemical properties of aqueous batteries. In this review, we describe the optimization strategies and mechanisms to provide guidance to future research on high-concentration electrolytes (HCE) and the challenge of high-energy and wide-temperature-range applications.

1 | Introduction

Aqueous batteries have garnered considerable attention due to good inherent safety, cost-effectiveness, and environmental sustainability [1–10]. In energy storage systems (EESs), although electrolytes are not directly engaged in electrochemical reactions, they are indispensable and affect the battery functionality [11]. The narrow electrochemical stability window (ESW) of water (1.23 V) in aqueous batteries constrains the operational voltage and energy density. Suo and colleagues have introduced a WISE to expand the operating potential window of aqueous batteries to 3.0 Vs [12]. Water-in-salt (WIS) and water-in-bisalt (WIBS) can decrease the number of free water molecules and form a solid electrolyte interphase (SEI) to minimize the SEI solubility in the electrolyte. However, the research on high-concentration aqueous electrolytes still faces problems such as high water activity, a

Summary

- This review summarizes the latest research on the improvements of aqueous batteries, provides high-concentration aqueous electrolyte optimization strategies, and reveals the electrochemical deteriorating mechanism from a microscopic perspective.
- Solvation structure, hydrogen-bond network, and interphase component are the keys for optimizing aqueous electrolytes.
- Appropriate salt selection, suitable salt concentrations, high-dielectric polar solvents, and synergistic electrodes are effective cooperation strategies for advanced aqueous batteries.

narrow ESW, and insufficient interface stability [13]. It is urgent to renew the aqueous batteries industry with improved electrochemical performance, high safety, and low-cost alternatives [14]. These issues directly affect the electrolyte cycling life and energy density. A high content of free water molecules in aqueous electrolytes causes high water activity in electrolytes [15–18]. This can easily trigger HER and the OER, leading to electrode corrosion. Anions and cations form solvation shells by ion-dipole interactions. For example, small ions with a large charge density (such as Mg^{2+}, Li^{+}) have a stronger solvation effect to create a tight solvation shell. Strongly hydrated ions break the original hydrogen-bond network of the solvent by competing for hydrogen bonds, effectively reducing the content of hydrogen bonds between water molecules. This means that the appropriate salt and suitable salt concentration in the electrolyte modulate the solvation structure, size, and composition. However, high-concentration electrolytes (HCEs) inevitably have low ionic conductivity. The WIBS electrolyte achieves a low concentration of aqueous electrolyte by combining two salts to avoid this problem. It also reduces free water in the mixed system and increases the stability of the electrolyte during the redox process. Furthermore, the role of the solvent in the electrolyte cannot be ignored. Polar solvents usually have a high dielectric constant, which promotes the dissociation of salts and the formation of fully solvated ions. The additive strategy is a simple and effective modification strategy. The types and concentrations of solutes and solvents regulate the solvent structure and ionic behavior of electrolytes, thereby expanding the voltage window and optimizing electrochemical performance [19–21]. Solvent addition reconstitutes the electrolyte dynamic structure, and a small amount of electrolyte additives can regulate the composition of the SEI and cathode electrolyte interphase (CEI). Therefore, researchers have developed strategies such as adding different salts, polar solvents, and ionic liquids to regulate the structure of the electrolyte [22–24]. Moreover, ion transport, interphase layer formation, and electrochemical properties depend on the electrode structure in battery systems.

To address the high water activity, narrow electrochemical window, and insufficient interface stability, the proper selection and combination of salts and solvents in water-in-salt electrolytes (WISE), double WISE, multi-salt hydrated electrolytes, and cosolvent electrolytes are important. In this review, we describe the selection of appropriate salts and modulation of their combinations to alter the solvation structure and hydrogen-bond network of WISE and reduce the occurrence of harmful interfacial side reactions. The augmentation of the electrochemical window is intricately associated with the solvation architecture and hydrogen-bonding network and is subject to their concerted regulation. Incorporating polar solvents and other additives into the electrolyte efficiently facilitates the formation of the SEI and the CEI [25, 26]. Certain modified electrolytes deliver exceptional performance with regard to energy density, electrode compatibility, and stable cycling characteristics. The proper electrolyte and electrode coordination optimizes the performance of aqueous batteries and expands the scope of practical applications.

2 | Fundamental Principles

Aqueous electrolytes have received extensive attention due to their high security and cost-effectiveness. However, their relatively narrow ESW (1.23 V) hampers development and applications. Dahn and colleagues have prepared a complete aqueous lithium-ion battery (ALIB) with spinel $LiMn_2O_4$ as the cathode and VO_2 as the anode in a 5 M $LiNO_3$ + 0.001 M LiOH aqueous electrolyte [27]. The battery inhibits hydrogen evolution and reduces the reduction potential of water by increasing the electrolyte pH with LiOH. However, the total electrochemical window does not change and the energy density of the battery does not increase. Consequently, an electrolyte with a broad ESW is imperative in order to substantially augment the energy density and voltage of aqueous battery systems [28].

In aqueous batteries, the decomposition voltage of salts is much lower than that of water. Therefore, water decomposes before salts, and the hydrogen evolution reaction (HER) and oxygen evolution reaction (OER) occur to aggravate the difficulty of forming a stabilized SEI interface [29]. HCEs proposed by Suo and colleagues expand the electrochemical window (Figure 1a) [12]. Adding salts, ionic liquids, polar solvents, etc. can modify the electrolyte and enhance the electrochemical properties (Figure 1b,c) [26]. Currently, there is no additive formulation that is applicable to all aqueous electrolytes. A HCE can indeed broaden the ESW and promote the formation of the SEI. However, the generation of ion pairs at high concentrations will increase the viscosity of the electrolyte and reduce the ionic conductivity. As a solvent with a high dielectric constant, water endows the aqueous electrolyte with a higher ionic conductivity than that of a nonaqueous electrolyte. An increase in salt concentration to a certain extent will promote the increase in ionic conductivity. Nevertheless, when the salt concentration continues to increase, the formation of ion pairs becomes an important factor affecting the ionic conductivity. These ion pairs cannot contribute to the ionic current and may even offset part of the ionic current, thereby reducing the ionic conductivity (Figure S1) [32]. This does not mean that ultra-high concentration aqueous electrolytes cannot have good ionic conductivity. For example, when the concentration of lithium trifluoromethanesulfonate (LiTFSI) is 21 M, the lithium-ion conductivity of WISE is still ~10 mS cm^{-1}. This is because the dissolved ions can form a three-dimensional ionic network that enhances conductivity in WISE to facilitate ion transport [33].

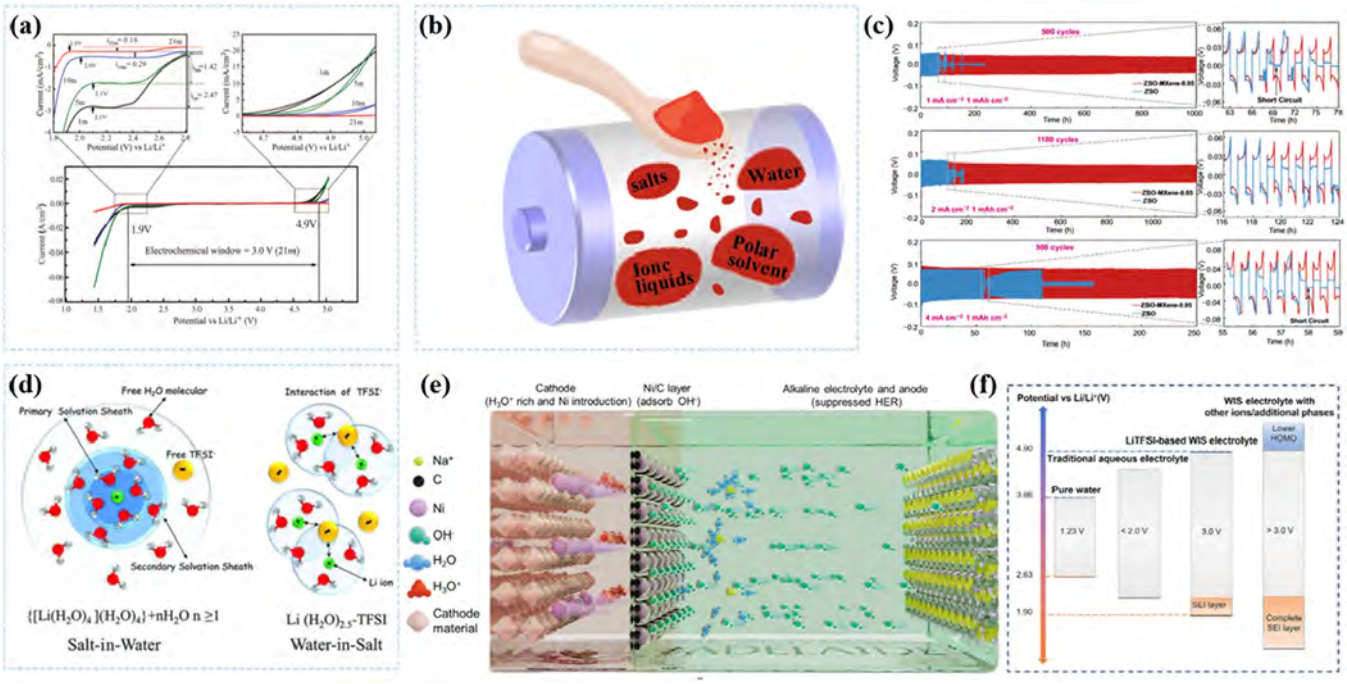

FIGURE 1 | Development and principles of high-concentration aqueous electrolytes. (a) The electrochemical stability window of LiTFSI–H_2O electrolytes on nonactive electrodes. Reproduced with permission: Copyright 2015, AAAS [12]. (b) Different addition strategies in aqueous electrolytes. (c) Long-term galvanostatic cycling of Zn–Zn symmetrical cell at 1, 2, and 4 mA cm^{-2} with the capacity of 1 mAh cm^{-2}. Reproduced with permission: Copyright 2021, Springer [26]. (d) Illustration of the evolution of the Li^+ primary solvation sheath in diluted and water-in-salt solutions. Reproduced with permission: Copyright 2015, AAAS [12]. (e) Design concept for the alkaline aqueous battery. Reproduced with permission: Copyright 2024, Springer Nature [30]. (f) Relation between the potential windows of pure water, traditional aqueous electrolyte, LiTFSI-based WIS electrolyte, and WIS electrolyte with other ions/additional phases. Reproduced with permission: Copyright 2022, Elsevier [31].

Zhao and colleagues added low-concentration $ZnSO_4$ to high-concentration lithium salts to supply Zn^{2+} required for zinc battery reactions, avoiding electrolyte viscosity increase or ion conduction obstruction caused by excessive Zn^{2+}. This study confirms the feasibility of "water-in-salt" in zinc batteries [34]. The Li^+ solvation sheath structure and the bulk electrolyte liquid structure are significantly changed compared to the low-concentration electrolyte, resulting in a widened ESW and altered interfacial chemistry on the cathode/anode [35]. Concentrated electrolytic solutions such as WISE constitute one of the effective strategies to mitigate HER [36]. In such electrolyte systems, there is a considerable presence of contact ion pairs, and the high salt concentration helps disrupt the H-bond network of water [37, 38].

In aqueous electrolytes, metal cations are more likely to combine with water molecules to form larger hydrated metal ions with a strong solvent sheath layer. As shown in Figure 1d [12], in lithium-ion aqueous batteries, Li^+ forms a strong solvated sheath structure with four water molecules in lithium-ion batteries. Generally, it is believed that a two-layer solvation structure is sufficient to shield the electric field of Li^+. Therefore, when the molar ratio of lithium ions to water is $Li:H_2O > 1:4$, there is a large amount of free water in the solvent. With increasing salt concentration and when the molar ratio of lithium ions to water is $Li:H_2O << 1:4$, there is no free water in the solvent. Since there is not enough water to shield the electric field of lithium, anions and cations will interact to form polymerized ion pairs, LiTFSI, and the electrochemical window widens.

HER can be suppressed by increasing the pH. To reduce HER, the alkaline fluorine-free sodium perchlorate electrolyte costs less than the common high-concentration salt electrolyte. Wu and colleagues have coated Ni/C nanoparticles on the NMF cathode to reduce HER and electrode dissolution (Figure 1e) [30]. However, the highly acidic or alkaline electrolyte with strong corrosiveness is inappropriate for large-scale applications [39–41]. Therefore, the formation of SEI passivation to offer kinetic protection against HER is much more effective and feasible [42]. On the heels of recent research on aqueous electrolytes, the electrochemical windows have expanded to be wider than 3 V (Figure 1f) [31].

3 | Aqueous Electrolytes With High Concentrations

3.1 | Water-in-Salt

The electrochemical mechanisms of aqueous batteries are almost the same as those of traditional organic batteries. However, the ion insertion/extraction reaction in aqueous electrolyte batteries is more complex. The typical salts used in WIS electrolytes are bis (trifluoromethylsulphonyl)imide ($TFSI^-$) [43], sodium trifluoromethanesulfonate (NaOTf) [44], sodium bis(fluoro sulfonyl) imide (NaFSI) [45], and potassium trifluoromethanesulfonate (KOTf) [46]. In addition, low-cost fluorine-free salts have also received extensive attention. Side reactions of electrode materials are prone to occur in aqueous batteries to affect the cycling stability of aqueous batteries. Irreversible proton coinsertion and

electrode dissolution compromise the performance and cycling life of aqueous batteries (Figure 2a) [50, 51]. Therefore, the proper match between high-concentration aqueous electrolytes and electrode materials is instrumental to the electrochemical performance of batteries. Electrode materials with high energy densities, wide ESWs, and good cycling characteristics are desirable.

3.1.1 | Anode Materials

Metal-based electrodes in aqueous batteries are a potentially viable solution for large-scale sustainable energy storage. These batteries have good safety, cost-effectiveness, and environmental friendliness (Table S1) [52, 53]. However, severe side reactions often occur on the electrodes of traditional aqueous batteries. Uncontrolled deposition in the subsequent deposition/dissolution cycle process produces the tip effects. When dendrites on the metal surface accumulate and grow, the separator may be penetrated, resulting in an internal short circuit in the battery [54]. Furthermore, the emergence of dendrites leads to an augmented contact area between the electrode and the electrolyte to intensify side reactions. During the deposition and dissolution processes, the cathode is also prone to side reactions, including HER and corrosion reactions [55]. Dendrite growth and side reactions usually occur simultaneously and affect each other. This vicious cycle has an irreparable impact on the cycling life and stability of the battery [56]. In HCEs, the strong solvation effect of cations causes free water and anions to enter the solvation structure, inducing anions to preferentially undergo reduction reactions on the electrode surface and deposit directionally to form a thin and dense SEI film. This reduces interfacial impedance and significantly improves battery interface stability.

For inorganic compound anodes, a good structure is conducive to the transportation of metal ions. Among them, $NaTi_2(PO_4)_3$ and $Na_3V_2(PO_4)_3$ have the 3D framework (Figure 2b and Figure S2) [47, 57–59]. For nonmetallic elements, the relatively high potential of sulfur can avoid the formation of an interphase layer rich in organic components due to the reduction of organic solvents. Batteries with elemental sulfur as the anode show good cycle stability (Figure 2c) [48, 60–63]. The proper electrodes and salts in electrolytes play a crucial role in forming the SEI film.

The electrolyte additive strategy is promising because it can avoid complex preparation processes, excessive ineffective weight, and high manufacturing costs [64]. A trace amount of electrolyte additive can effectively improve the stability of the SEI in the battery. The modification strategy is inexpensive, easy to operate, and suitable for large-scale energy storage [65]. For example, strong Li^+-solvating salts are added to the polymer electrolyte of $ZnSO_4$ to reduce the freezing temperature of the electrolyte, improve the performance of the electrolyte at a low temperature, and expand the operating temperature range. The metal ions adsorb onto the anode surface to inhibit interfacial side reactions and facilitate the uniform deposition of Zn (Figure 2d) [66]. The addition of long-chain polyethylene oxide polymer (PEO) can produce uniform deposition of Zn and inhibit the transfer of Zn^{2+} ions to enhance the cycling life and electrochemical properties of the electrode (Figure S3). The suppressed transfer kinetics of Zn^{2+} ions and the uniform distribution of Zn^{2+} ions at the interface contribute to the uniform deposition-dissolution process of Zn. The addition of ether groups adjusts the ion concentration on the anode interface and the viscosity of the electrolyte (Figure 2e) [67]. In addition, the influence of the separator on the performance of high-concentration aqueous batteries cannot be ignored. For example, the introduction of an under-liquid dual super-lyophobic membrane-based separator enables the separation of electrolytes, avoiding the penetration of catholyte to the anode and irreversible electrode corrosion (Figure 2f) [49, 68].

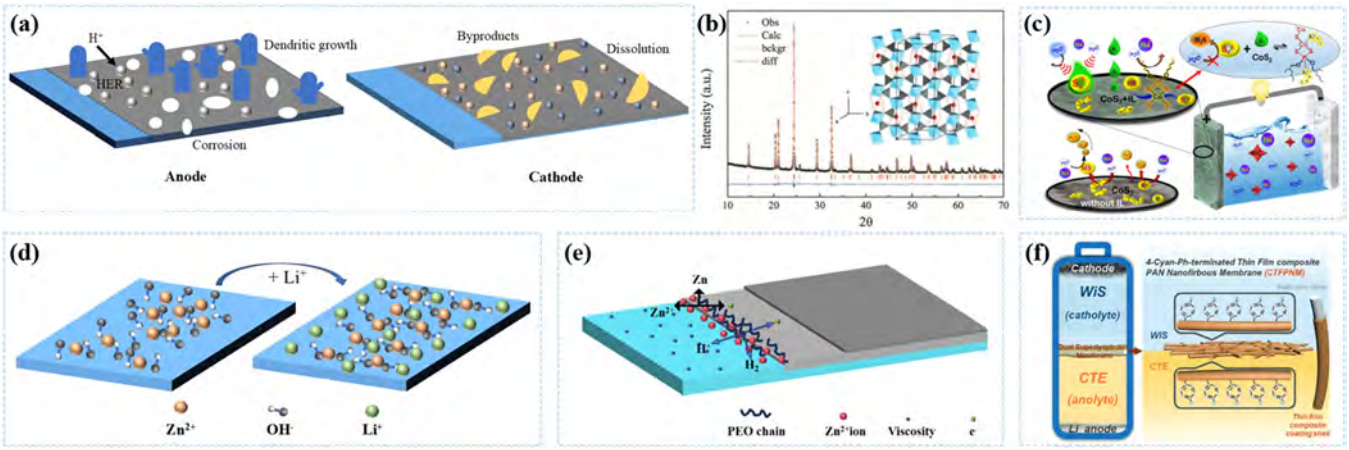

FIGURE 2 | Mechanisms of side reactions and modification methods on anodes in aqueous batteries. (a) Schematic illustration to describe side reactions in aqueous batteries. (b) Rietveld refinement of the X-ray diffraction pattern of as-synthesized NTP and schematic illustration of crystal structure. Reproduced with permission: Copyright 2013, Wiley-VCH [47]. (c) Schematic representation of polysulfide interaction at S@CoS2 anode in the presence and absence of ionic liquid in aqueous Na-ion/S battery. Reproduced with permission: Copyright 2022, Elsevier [48]. (d) Schematic illustration of the interfacial reactivity in Z-PAAm and ZL-PAAm. (e) PEO polymer molecules stabilizing Zn anode reactions by slowing down Zn^{2+} ions transfer kinetics, regulating Zn^{2+} ions concentration, and smoothing the surface chemistry at the vicinity of Zn anode, leading to smooth Zn deposition and suppressed hydrogen generation PEO. (f) Introduction of under-liquid dual super-lyophobic membrane-based separator into the hybrid-electrolytes system. Reproduced with permission: Copyright 2024, Wiley-VCH [49].

3.1.2 | Cathode Materials

Significant progress has been made for aqueous electrolytes and cathode materials such as metal oxides [47, 69, 70], polyanions [71, 72], Prussian blue analogs [73–75], and transition metal oxides [76] with excellent cycling and rate properties [77]. Compared with low-concentration electrolytes, the metal-ion solvation sheath structure, and electrolyte liquid structure in HCEs exhibit significant changes, resulting in a widened ESW and changes in the interfacial chemical properties of the cathode and anode. The CEI is a film formed by the decomposition of the electrolyte on the cathode surface [78]. Modifying the electrolyte can regulate the composition of the CEI layer, enhance ion transfer kinetics, and reduce harmful interfacial side reactions, achieving a stable electrolyte interface (Figure 3a) [79, 84].

It is well known that polar groups in polar organic solvents can alter the solvation structure of metal ions in the electrolyte [85]. Zhang and colleagues have developed battery systems with a distinct H^+/OH^- dissociation mechanism based on the amphoteric aluminum hydroxyacetate ($AlAc(OH)_2$) electrolyte. Since the H^+/OH^- dissociation ability with dissociation constants of 5.0/3.0 is stronger than that of water (14.0), it can stabilize the redox reaction of the electrode (Figure 3b and Figure S4). The absorption of H^+ prevents the formation of ionic bonds at the AQ anode and inhibits the dissolution of the electrode, while the local alkaline environment provided by OH^- for the stable conversion reaction of the $Ni(OH)_2$ cathode can enhance the cycling stability and reversibility of the $Ni(OH)_2$ cathode [80].

Electrode materials selection cannot ignore the influence of insertion/extraction ions. The radius of the ions influences the structure of cathode materials. The radius of hydrated Na^+ ions is relatively small. Therefore, after insertion into the cathode of $FeFe(CN)_6$, it can still maintain a cubic structure with lattice changes and show good electrochemical properties. However, the radius of hydrated Li^+ ions is relatively large, thus causing large structure deformation (Figure 3c) [81]. Hydrogel electrolytes possess unique microporous structures and chemical compositions. With the rapid development of flexible materials and wearable electronic materials, hydrogel electrolytes are advancing toward flexible energy, and the exploration of hydrogel synthesis processes is becoming increasingly mature [86]. Zhang and colleagues have utilized hydrogen bonds in the topological network to restrict active water molecules in the hydrogel network to enhance the hydrogen bonds between the gel network and water molecules (Figure 3d) [82]. Hydrogel electrolytes have superior ionic transport properties compared to traditional electrolytes, and their cross-linked structure also facilitates water retention (Figure 3e and Figure S5) [83, 87]. Solid-state electrolytes also represent a non-negligible component, Chi and colleagues design a zeolite membrane-based solid electrolyte (GS-ZM) by introducing $LiTFSI^-$-based guest species into the supercages of LiX zeolite, where the "oxygen wrench" of $TFSI^-$ dynamically coordinates with framework Li^+ to activate lithium ion conduction, achieving both high ionic conductivity and interfacial compatibility [88].

3.2 | Water-in-Bisalt

In the aforementioned WISE, the ESW is broadened. However, the width of the ESW of the WISE cannot break the solubility limit of the selected salt. Adding a supporting salt to the WISE is a feasible scheme. The WIBS electrolyte promotes the energy density and ESW of aqueous batteries with two salts [89].

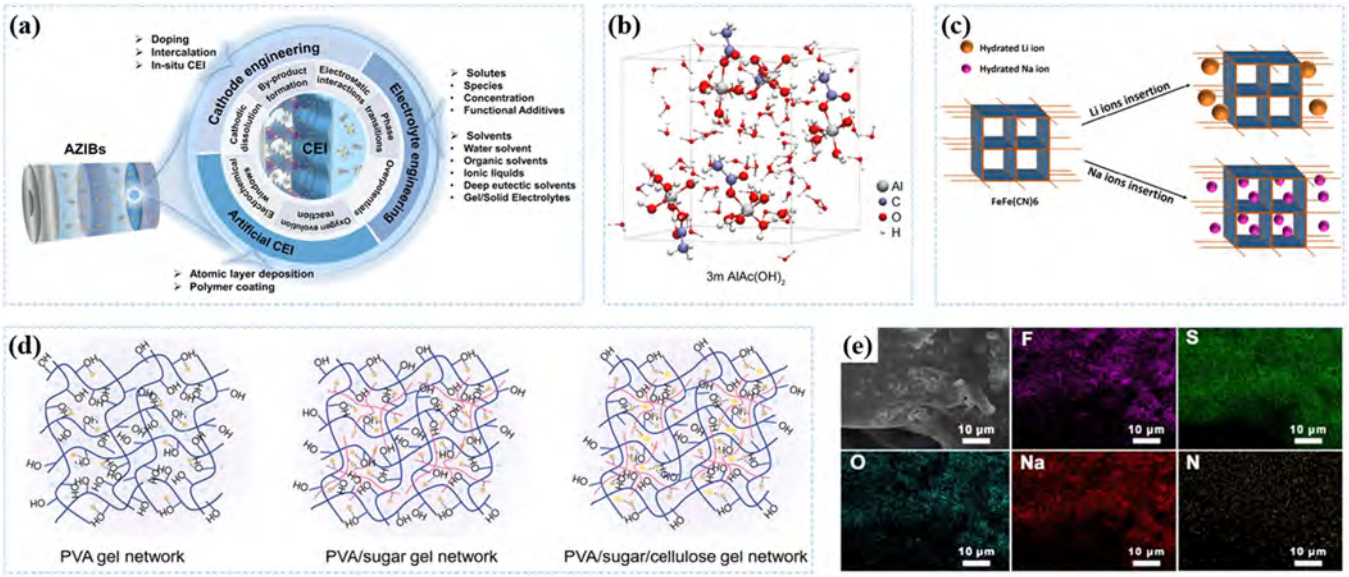

FIGURE 3 | Challenges and regulation strategies of the catholyte interface. (a) Schematic illustration of challenges at the CEI in AZIBs and strategies for addressing the challenges. Reproduced with permission: Copyright 2024, JEC [79]. (b) The snapshot of the molecular dynamics of 3 M $AlAc(OH)_2$ electrolyte. Reproduced with permission: Copyright 2024, American Chemical Society [80]. (c) Investigation of iron hexacyanoferrate as a high-rate cathode for aqueous batteries: Sodium-ion batteries and lithium-ion batteries. Reproduced with permission: Copyright 2018, Elsevier [81]. (d) Schematic diagram of PVA gel network, PVA-S gel network, and PVA-S-C gel network. Reproduced with permission: Copyright 2024, Wiley-VCH [82]. (e) Elemental maps of the F, S, O, Na, and N of a typical polyacrylamide hydrogel film. Reproduced with permission: Copyright 2018, American Chemical Society [83].

By choosing the appropriate supporting salt, researchers have widened the ESW further to allow the battery to operate at a higher voltage [90]. In the aqueous electrolyte system, the introduction of supporting salts can significantly alter the solvation structure, hydrogen-bond network, and interfacial components. When selecting salts, cationic salts with strong solvation ability and anions that contribute to the construction of the SEI are taken into consideration. Additionally, additive salts containing polar functional groups can form hydrogen bonds with water molecules, thus changing the hydrogen-bond network. The addition of ionic liquids can increase the solubility of salts and enhance the conductivity of the electrolyte. Ionic liquids can also act synergistically with other components to improve the diverse properties of high-concentration aqueous electrolytes, meeting the requirements of different application scenarios.

Fluorinated electrolytes are common electrolytes in industrial processes. However, the high cost of fluorinated salts causes problems in commercialization. Researchers have tried to use fluorine-free salts to produce similar effects as fluorinated salts and reduce the cost of fluorinated salt aqueous batteries. Double-salt aqueous electrolytes can be divided into fluorinated salt electrolytes and fluorine-free salt electrolytes. In aqueous batteries, the solvation structure of metal ions is important and affects the properties of the electrolyte [91]. The coordinated water molecules of metal ions migrate to the anode surface along with the metal ions for the HER [51]. During this process, the pH of the electrode surface changes to promote the growth of dendrites [92]. By optimizing the solvation structure of metal ions and reducing the content of free active water in the electrolyte, these deleterious electrode side reactions can be mitigated [93, 94].

3.2.1 | Fluoride-Containing Salts

Fluorine has more vigorous oxidation activity than oxygen and is not easily oxidized by oxygen. The fluorine-rich layer formed by the decomposition of fluorine-containing salt electrolytes can passivate the electrode-electrolyte interface, inhibit the HER, and increase the electrochemical window of the electrolyte to achieve long-term cycling. This strategy has been considered the key to preparing high-performance aqueous batteries [95]. Introducing supporting salts into fluorine-containing aqueous electrolytes can change the solvation structure to produce better properties. Taking bis(trifluoromethane sulfonyl)imide ($TFSI^-$) as an example, as shown in (Figure 4a), by adding 7 M LiOTf to a 21 M LiTFSI solution, an average of 0.5 water molecules can be replaced from the solvation shell to change the solvation structure of metals. The decrease in free water molecule fraction in WIBS compared with that in WIS increases ESW in the concentrated electrolyte (Figure 4b) [89]. In the neutral WIBS electrolyte prepared by Tang and colleagues consisting of 20 M LiTFSI and 2 M $Al(OTf)_3$, $TFSI^-$ is forced to enter near the cation to form a contact ion pair $(Al\text{-}TFSI)^{2+}$ and suppress the presence of $(Al\text{-}(H_2O)_6)^{3+}$ (Figure 4e and Figure S6) [97]. The unique solvation sheath structure of the Al^{3+} cation can protect the Al metal anode from corrosion and eliminate the

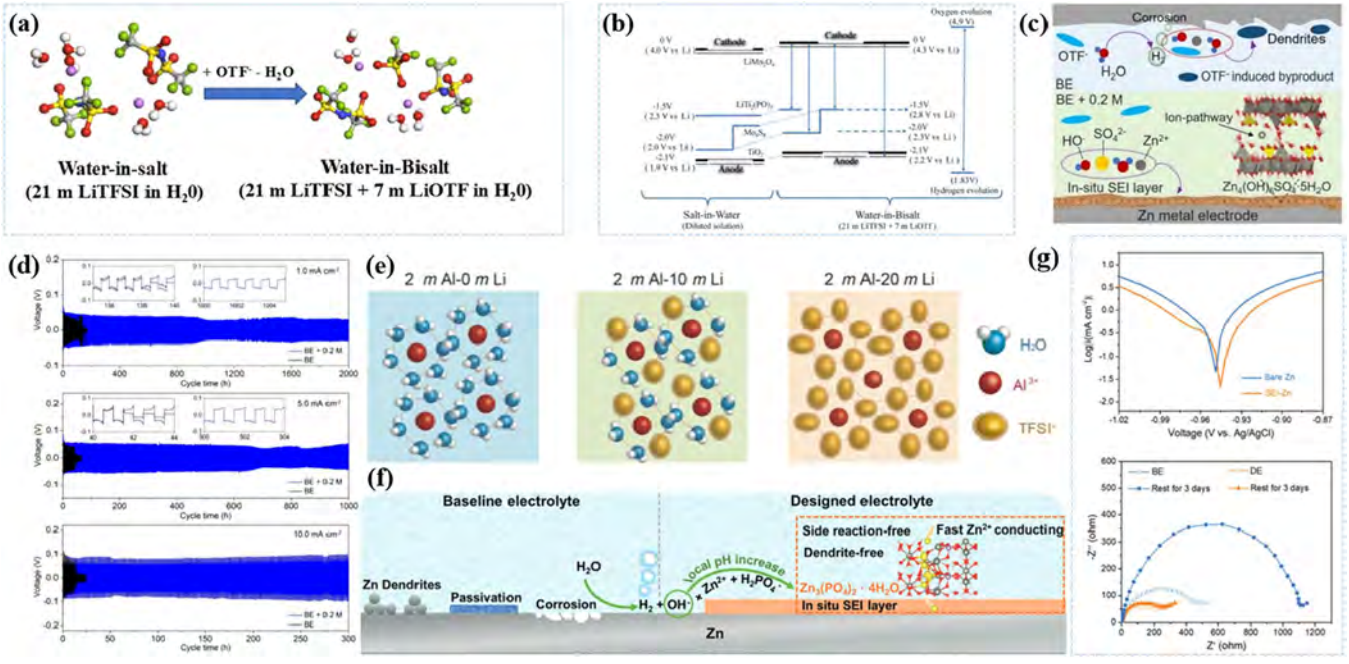

FIGURE 4 | Salt synergistic effects in dual-salt electrolytes. (a) Schematic representation of the influence of the addition of 7 M LiOTf on the solvate structure and the composition of the Li^+ first coordination shell extracted from MD simulations. (b) Output voltages generated by established. Reproduced with permission: Copyright 2016, Wiley-VCH [89]. (c) In-situ formation and characterization of SEI on Zn. Reproduced with permission: Copyright 2022, Elsevier [96]. (d) Electrochemical performance and morphological characterization of Zn electrodes in BE with/without 0.2 M $ZnSO_4$ additives. Cycling performances of symmetric Zn||Zn cells under 1.0, 5.0, and 10.0 mA cm^{-2}. Reproduced with permission: Copyright 2022, Elsevier [96]. (e) Schematic diagram of LiTFSI concentration effect on Al^{3+} solvation-sheath structure. Reproduced with permission: Copyright 2024, Elsevier [97]. (f) Schematic illustration of Zn surface evolution and the SEI formation mechanism. Reproduced with permission: Copyright 2021, Wiley-VCH [98]. (g) Interfacial stability and Zn-ion transport property of the in situ SEI layer. Reproduced with permission: Copyright 2021, Wiley-VCH [98].

HER to improve the reversibility of the Al metal anode. The reasonable selection and combination of two salts in the double-salt WISE can widen the electrochemical window and inhibit or even eliminate adverse side reactions.

In addition to the above strategy in which two fluorine-containing salts act in concert, a modification strategy has been proposed. Adding nonfluoride salts as supporting salts in fluoride salt electrolytes can also solve the problems of side reactions and ESWs [99]. The $ZnSO_4$ aqueous electrolyte has high stability and excellent compatibility with cathode materials and is environmentally friendly, low-cost, and a widely recognized electrolyte. In the fluorine-containing dilute solution, a supporting salt is added to introduce SO_4^{2-} ions, the SO_4^{2-} ions with strong coordination ability replace OTF^- to enter the solvation shell of zinc ions, and a dense SEI, $Zn_4(OH)_6SO_4{\cdot}5H_2O$, is generated on the electrode. The tunnel structure of $Zn_4(OH)_6SO_4{\cdot}5H_2O$ provides channels for ion diffusion, ensuring high ionic conductivity (Figure 4c). The performance of Zn || Zn batteries has been significantly improved. The irreversible problems faced by zinc anodes in the reference electrolyte include continuous HER, dendrite growth, and corrosion, which can be restrained (Figure 4d) [96]. Zeng and colleagues have added $Zn(H_2PO_4)_2$ to the electrolyte and utilized the OH^- generated during HER in the electrolyte to promote the formation of the SEI composed of $Zn_3(PO_4)_2{\cdot}4H_2O$ (Figure 4f). The SEI film inhibits further electrode side reactions. Moreover, its high ion transference number and Zn^{2+} promote the uniform deposition of metal ions (Figure 4g) [98].

The addition of $(NO_3)^-$ additives to the WIS electrolyte is also beneficial to the construction of a protective SEI layer. The presence of two salts often implies more complex SEI components, Li and colleagues have designed a bilayer SEI consisting of a robust inorganic ZnF_2–$Zn_5(CO_3)_2(OH)_6$ layer and an organic layer formed in situ in a low-concentration aqueous $Zn(OTf)_2$–$Zn(NO_3)_2$ electrolyte to prevent water penetration and stop hydrogen evolution during zinc plating/stripping in Zn symmetric cells (Figure 5a and Figure S7) [100]. The two salts in the WIBS electrolyte widen the ESW. Jin and colleagues have designed an economical 19 M bisalt WISE with a wide ESW of 2.8 V. The low-cost 17 M $NaClO_4$ extends the anodic limiting potential to 4.4 V, while the fluorine-containing salt (2 m NaOTf) extends the cathodic limiting potential to 1.6 V by forming the NaF–Na_2O–NaOH SEI on the anode (Figure 5b and Figure S8) [101]. This hybrid SEI is formed through the synergistic effect of dual salts. $NaClO_4$ reduces water activity and free water content, allowing the OTF^- ions of the supporting salt to participate in the solvation shell containing ClO_4^- and

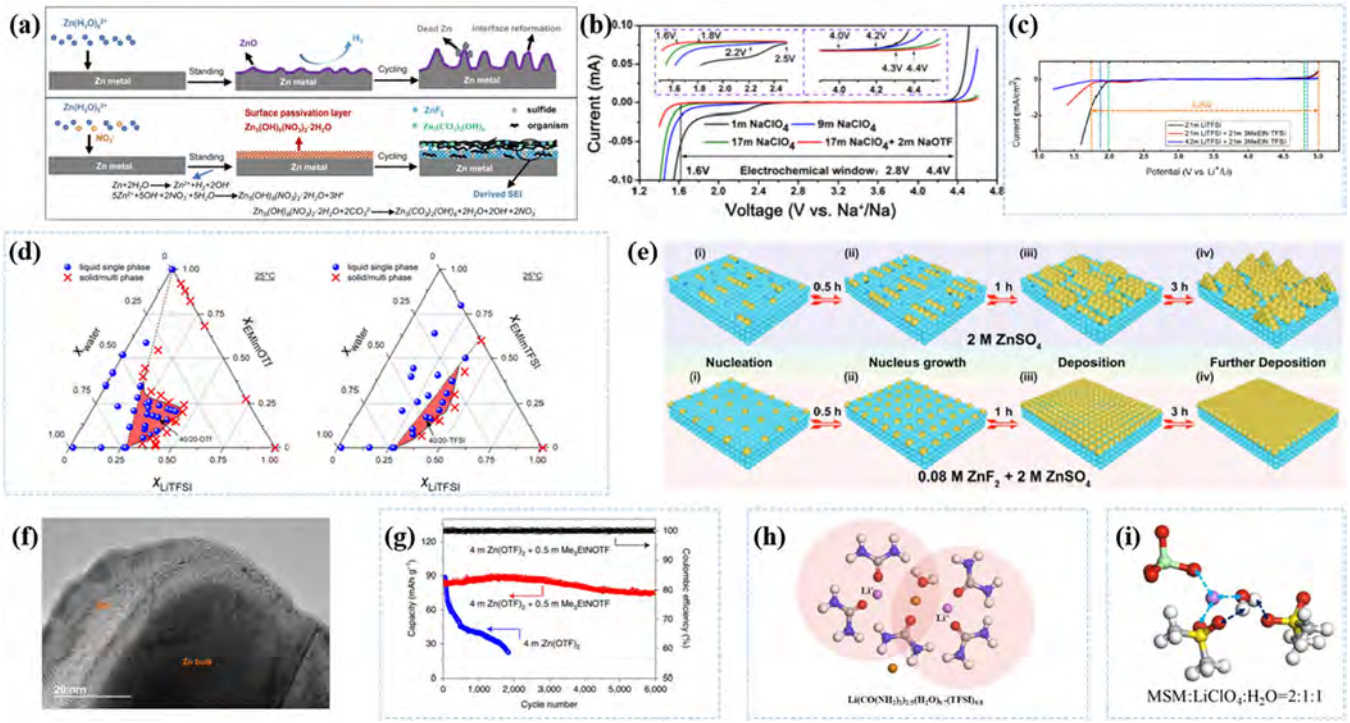

FIGURE 5 | Modification strategies of fluoride-containing salt electrolytes. (a) Illustration of surface evolution mechanism. Reproduced with permission: Copyright 2021, Wiley-VCH [100]. (b) Solvation structure and property of $NaClO_4$–NaOTf–H_2O electrolytes. Reproduced with permission: Copyright 2021, Wiley-VCH [101]. (c) Electrochemical windows of different aqueous electrolytes as measured on the inactive current collector (stainless steel) at a scanning rate of 5 mV s^{-1}. Reproduced with permission: Copyright 2020, American Chemical Society [102]. (d) Ternary phase diagrams of LiTFSI/RTIL/water mixtures at 25°C with EMImOTf and EMImTFSI as the RTIL. Reproduced with permission: Copyright 2021, Wiley-VCH [103]. (e) Schematic diagrams and morphology evolutions for stainless steel substrate deposited Zn at different electrolytes. Reproduced with permission: Copyright 2021, Wiley-VCH [104]. (f) TEM image for Zn metal interphase obtained from Zn||Zn symmetric cells with 4 m $Zn(TFSI)_2$ + 4 m Me_3EtN–TFSI in H_2O after 80 h of cycling (0.5 mA cm^{-2}, 0.5 mAh cm^{-2}) at room temperature. Reproduced with permission: Copyright 2022, Cell Press [105]. (g) Rate performance of the Zn||$VOPO_4$ coin cell in different electrolytes at 2.0 A g^{-1}. Reproduced with permission: Copyright 2021, Springer Nature [106]. (h) Illustration of the Li^+ primary solvation shell in the 4.5 m electrolyte. (i) Liquid structure of MSM:Li-ClO_4:H_2O = 2:1:1 DES electrolyte calculated from DFT.

water molecules, further inhibiting water decomposition and creating a favorable environment for the formation of a stable SEI film. NaOTF reacts on the anode surface to form a composite SEI layer with ionic conductivity, mechanical strength, and hydrophobic barrier functions.

Raman scattering and nuclear magnetic resonance (NMR) reveal that the hydrophilic effects of ionic liquids can increase the solubility of fluorinated salts. Becker and colleagues have reduced the molar ratio of lithium ions to water to 1.39 and pushed the content of LiTFSI to the solubility limit (Figure 5d) [103]. Wang and colleagues have changed the solvation sheath structure of Li^+ by introducing non-lithium co-salts into the fluorinated salt aqueous electrolyte. This 63 M aqueous electrolyte (42 M LiTFSI + 21 M $Me_3EtN{\cdot}TFSI$) provides a wide potential window of 3.25 V (Figure 5c), and the symmetrical ammonium salt exists as a supporting salt and doubles the solubility of LiTFSI. The WIBS electrolyte supports a 2.5 V ALIB, which provides a high energy density of 145 Wh $kg^{-1,}$ and is stable for more than 150 cycles (Figure S9) [102]. Me_3EtN–TFSI as a supporting salt can also form a unique SEI film on the anode to improve the reversibility of the zinc anode. This is due to the formation of ZnF_2, $ZnCO_3$, and fluoropolymer species (Figure 5f) [105]. It is worth noting that the ZnF_2-rich SEI prevents water molecules from coming into contact with the electrode while allowing metal ions to pass through (Figure S10) [106]. ZnF_2 reduces the nucleation overpotential and plateau overpotential of zinc deposition and forms a fluorine-rich layer on the surface of the zinc anode. The hydrophobic ZnF_2 in the inner layer prevents direct contact between zinc and water, further removing solvated water and inhibiting water decomposition and the growth of Zn dendrites, while allowing Zn^{2+} to pass through, thus ensuring uniform deposition of Zn^{2+} and preventing HER (Figure 5e) [104]. Similarly, adding trimethylethyl ammonium trifluoromethanesulfonate ($Me_3EtNOTF$) to the aqueous electrolyte can improve the Coulombic efficiency (CE) of electrode plating/stripping (Figure 5g) [106].

Although salt addition increases the salt concentration in the electrolyte, the ionic conductivity of the electrolyte decreases. Therefore, low-concentration aqueous electrolytes are also considered [107]. The low-concentration ternary eutectic electrolyte of 4.5 M (LiTFSI)–KOH–$CO(NH_2)_2$–H_2O (Figure 5h) [108] and the mixture of BMITFSI, $Zn(TFSI)_2$ and water constitute a ternary deep-eutectic system with the melting point below −80°C (Figure S11) [109]. This improves the ESW of the electrolyte. Eutectic electrolytes, with good electrochemical and thermal stability, have attracted attention [110, 111]. From the microscopic perspective, the eutectic system is composed of closely associated ion pairs without free molecular components. This unique ionic network structure not only promotes the formation of a stable solid electrolyte interface (SEI) but also regulates the uniform deposition/dissolution process of the metal electrode, thus achieving highly reversible electrode reaction kinetics [112, 113]. In the hydrated eutectic system, all the water molecules are locked in the eutectic framework by hydrogen bonding. Compared with freely moving water molecules in ordinary aqueous electrolytes, the water molecules in the eutectic electrolyte are restricted by the hydrogen-bonding network (Figure 5i). This restricted coordination environment inhibits water decomposition side reactions and provides a wide voltage window similar to organic electrolytes while maintaining the safety advantages of aqueous systems [114].

3.2.2 | Fluorine-Free Electrolytes

Although LiTFSI-based WISEs are innovative, the high solubility of the SEI formed by fluorine-containing salts limits the battery lifespan, and the high concentration and cost of fluorine-containing salts pose challenges to their commercial viability. To reduce the cost associated with fluorine-containing WISEs, a viable approach is to use fluoride-free salt electrolytes to achieve similar effects. Acetates (potassium acetate, KOAc) or perchlorates are good choices [115]. Unlike simply increasing the salt concentration in a WIS electrolyte, adding concentrated supporting salts is another promising strategy to avoid the solvation of metal ions by water in aqueous solutions [116–118]. Deng and colleagues have designed a low-cost superconcentrated (SC) aqueous electrolyte with potassium acetate (KAc) and lithium acetate(LiAc). The high K^+ concentration confines water molecules by cation solvation, and the SC aqueous electrolyte improves the ESW (2.85 V) and capacity (Figure 6a) [125]. In addition, Han and colleagues have used a mixture of high-concentration sodium acetate (8 M) and potassium acetate (32 M) to inhibit the water activity [126].

Nitrate is a supporting salt and its addition to a fluorine-containing salt electrolyte can promote the formation of SEI and improve the electrochemical performance (Figure 6b and Figure S12) [119, 127]. It has promising applications in fluorine-free salt electrolytes. For example, a fluoride-free WIBS electrolyte composed of $LiNO_3{\cdot}3H_2O$ and $NaNO_3$ exhibits an ESW as large as 3.1 V boding well for large-scale energy storage (Figure 6c) [120]. Wang and colleagues have demonstrated that the addition of a small amount of magnesium sulfate ($MgSO_4$) can enhance the cycling life of the zinc sulfate ($ZnSO_4$) electrolyte. Electrostatic shielding formed on the electrode stems from the high adsorption energy between magnesium ions (Mg^{2+}) and the zinc electrode, thereby causing Mg^{2+} to preferentially adsorb on the anode over Zn^{2+}. Moreover, the high binding energy between Mg^{2+} and water molecules (H_2O) modifies the solvation structure of Zn^{2+}. Mg^{2+} and Zn^{2+} compete for the solvation of SO_4^{2-}, thus altering the solvation structure of Zn^{2+}. The change in the solvation structure further restricts water molecules (Figure 6d,e) [121]. The work discloses the effect of the SO_4^{2-} additive as a supporting salt in a fluorine-free double-salt aqueous electrolyte.

Similar to fluorine-containing WIBS electrolytes, in addition to the interaction between inorganic salts, ionic liquids can improve the electrochemical properties of aqueous batteries. Ionic liquids (ILs) possess excellent electrical conductivity and thermal stability but suffer from high costs [128]. In polymer electrolytes, the polymer network provides an orderly transmission channel for ions and reduces the transmission resistance of ions. At the same time, the polymer network can also fix salt ions to prevent them from precipitating from the electrolyte. Adding ionic liquids enhances the conductivity of the electrolyte and helps to form a more stable solid electrolyte interface, further improving the transmission efficiency of ions in polymer electrolytes [129]. Zhu and colleagues have

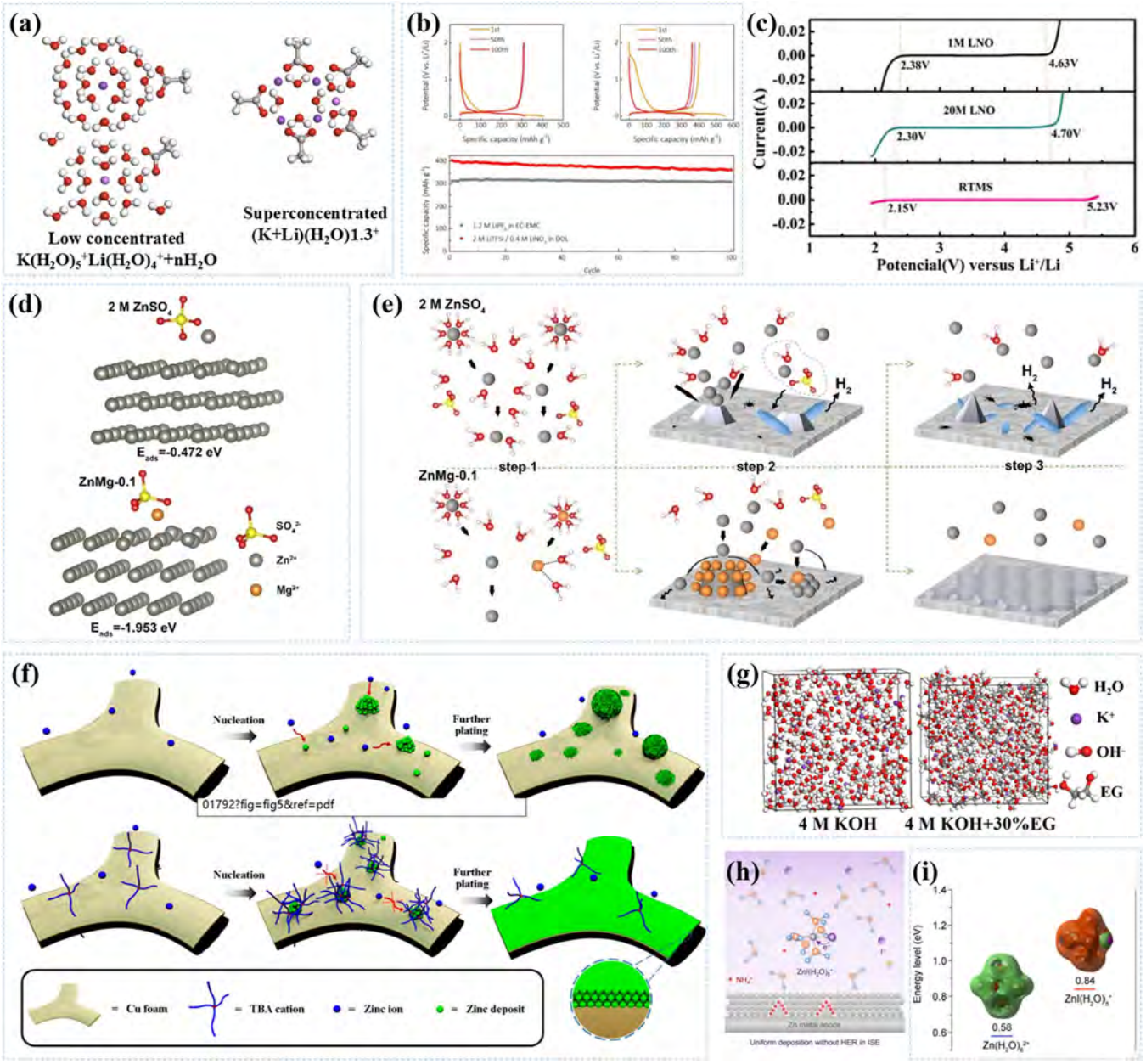

FIGURE 6 | Fluoride-free salt electrolytes can effectively inhibit side reactions. (a) Schematic illustration of the cation solvation of the SC and LC electrolytes. (b) Electrochemical performance of graphite anode in a traditional EC-based electrolyte and nanostructured electrolyte. Reproduced with permission: Copyright 2024, American Chemical Society [119]. (c) CV acquired in different electrolytes from titanium mesh working electrodes at 10 mV s^{-1}, where Li/Li^+ is the reference potential. Reproduced with permission: Copyright 2021, Wiley-VCH [120]. (d) Adsorption of electrolyte ions on a Zn surface and corresponding adsorption energy (Eads). Reproduced with permission: Copyright 2021, Wiley-VCH [117]. (e) Schematics of Zn deposition process in the 2 M $ZnSO_4$ (top row) and $ZnMg_{0.1}$ (bottom row) electrolyte. Reproduced with permission: Copyright 2021, Wiley-VCH [121]. (f) Schematic illustrations of Zn deposition on Cu foam without or with TBA_2SO_4 as an electrolyte additive. Reproduced with permission: Copyright 2020, American Chemical Society [122]. (g) MD simulations of the blank electrolyte and an electrolyte with 30% EG. ESP maps of used additives for morin. Reproduced with permission: Copyright 2020, Royal Society of Chemistry [123]. (h) Design strategy of I^- participating solvation structure electrolyte. Reproduced with permission: Copyright 2022, American Chemical Society [124]. (i) LUMO energy level of $Zn(H_2O)_6^{2+}$ and $ZnI(H_2O)^{5+}$. Reproduced with permission: Copyright 2022, American Chemical Society [124].

prepared an ionic liquid-ethylene glycol system to form a local concentrated-salt-solution electrolyte. The salt concentration is reduced by the synergistic effect between morin and the ionic liquid, leading to higher ionic conductivity. Experiments such as electrochemical tests, surface analysis, and theoretical calculations prove that the additives modulate the anodic interface and restrain the free water molecules through hydrogen bonding (Figure 6g) [128]. Polar solvents can also reduce the cost of ionic liquids and provide a new direction for the large-scale application of ionic liquids. Bayaguud and colleagues have demonstrated tetrabutylammonium sulfate (IL) as an electrolyte additive in an aqueous 2 M $ZnSO_4$ solution. Dendrite growth is hindered by changing the deposition direction of Zn cations on the interface (Figure 6f) [122, 123]. Halogen ions, as

stronger electron donors than water molecules, are more inclined to coordinating with transition metal ions [124]. The negatively charged halogen ions can transfer electrons to the original Zn^{2+} solvation structure. By inhibiting the reduction of the lowest unoccupied molecular orbital (LUMO) energy level, electron loss of water molecules in the solvation structure can be reduced to improve the reduction stability. Furthermore, many additives destroy the original hydrogen-bonding network and reduce the water–water interaction (Figure 6b,i and Figure S13) [130, 131].

3.3 | Multi-Salt Hydrated Electrolytes

Multi-salt aqueous electrolytes usually outperform WIBS electrolytes in terms of performance and stability by providing multiple ion choices and interactions. They can improve the efficiency and safety of batteries and other electrochemical devices in specific applications [132]. Regulating the inner solvation structure of electrolytes by incorporating higher donor number dual anion additives into the conventional electrolyte system gives rise to the active participation of dual anion additives in the inner solvation shell around the cation to influence the reductive stability of the pure solvent molecules and metal ion-solvent complex by raising their LUMO levels upon the introduction of anions (Figure 7a) [135].

The "hybrid aqueous/nonaqueous" electrolyte (HANE) is an innovative electrolyte system [136]. Introducing nonaqueous solvents and specific salts, on the basis of effectively reducing the flammability of organic components, broadens the ESW and provides better energy density and cycling lifespan. The hybrid aqueous/nonaqueous bisalt mixed electrolyte forms a denser and more stable SEI film on the cathode surface, which consists of LiF and alkyl carbonates. The F_{1s} signal reveals the presence of LiF as the main component, while the C_{1s} signal indicates the existence of alkyl carbonates. This effectively prevents the continuous decomposition of the electrolyte and improves the cycling stability of the battery (Figure 7b,c) [133, 134]. Zhu and colleagues have made a uniformly mixed hybrid aqueous/nonaqueous bisalt mixed electrolyte with 7 M LiOTf + 21 M LiTFSI aqueous solution and nonaqueous component LiTFSI in DMC. The CE of this battery is comparable to that of dual-ion batteries with nonaqueous organic electrolytes and can reach 93.9% (Figure 7d) [137]. In this electrolyte, the free water concentration is minimal. Therefore, it can be considered that $TFSI^-$, OTf^-, and DMC^- form a saturated solvated sheath structure with Li^+. The water activity of the mixed electrolyte is fully suppressed to improve the stable potential window.

3.4 | Cosolvents WIS Electrolytes

Chen and colleagues have proposed the "ether-in-water" electrolyte (EIWE) aqueous hybrid solvated electrolyte. Tetraethylene glycol dimethyl ether (TEGDME), with excellent interfacial stability, low viscosity, and high ionic conductivity, is selected as the cosolvent for aqueous batteries, to produce effective separation of anion–cation pairs in the electrolyte (Figure 8a,b) [142]. The basic design rule of a cosolvent WIS electrolyte is that the cosolvent forms a homogeneous phase with the WIS electrolyte. Two problems can be solved by adding cosolvents. On the one hand, the morphology of deposited metals is adjusted from large, fragile, and loosely stacked flakes to small and uniformly spherical particles to achieve dendrite-free deposition through cosolvents. On the other hand, the ability to prevent side reactions on metal anodes can be improved by cosolvents [143]. Furthermore, when considering the characteristics of cosolvents concerning parameters such as the dielectric constant and solvation strength, different properties of WIS electrolytes can be optimized by adjusting the ratio of cosolvents to achieve better battery performance.

Polar organic solvents are effective cosolvents, and they usually have high dielectric constants, including alcohols, esters, ketones, ethers, and amides [94, 139]. Polar organic solvents into fluorine-containing salt electrolytes and fluorine-free salt electrolytes can both weaken the dipole interaction of metal ions,

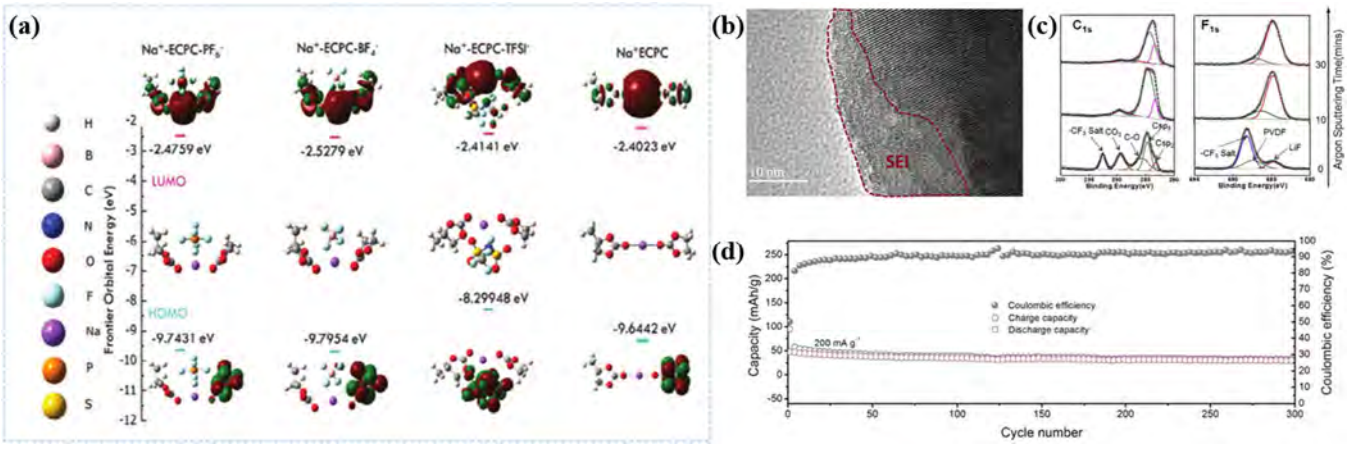

FIGURE 7 | Multi-ion synergistic effects and interface chemical regulation in multi-salt water-in-salt electrolytes. (a) HOMO-LUMO energy levels for Na^+-solvent anion complexes and Na^+-solvent complex. Reproduced with permission: Copyright 2024, Elsevier [132]. (b) X-ray photoelectron spectroscopy (XPS) and (c) transmission electron microscopy image of fully lithiated LTO electrodes. The cells were charged at 3.5 V before LTO was recovered, and the XPS depth profile was acquired by Ar^+ sputtering. SEI, solid-electrolyte interphase. Reproduced with permission: Copyright 2018, Elsevier [133]. (d) Cycling stability test at 200 mA g^{-1} for 300 cycles. Reproduced with permission: Copyright 2018, Elsevier [134].

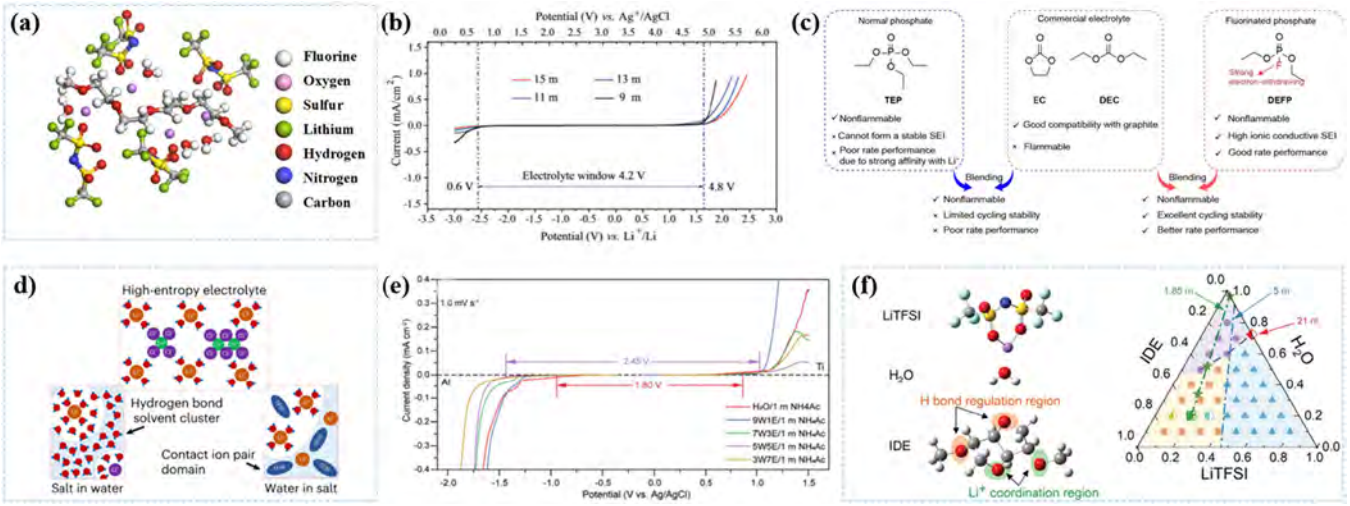

FIGURE 8 | Modification strategies of cosolvent additives. (a) A schematic of the EIWE and the composition of the Li^+ first coordination shell extracted from AIMD simulations with a focus on oxygen atoms. (b) Electrochemical stability window of four different EIWEs with cyclic voltammetry (CV). Reproduced with permission: Copyright 2020, Wiley-VCH [137]. (c) Design concepts and molecular characteristics of DEFP. Reproduced with permission: Copyright 2023, Springer Nature [138]. (d) Illustration of solution structure in different electrolytes. Reproduced with permission: Copyright 2022, Royal Society of Chemistry [139]. (e) ESW of various electrolytes determined by LSV. Reproduced with permission: Copyright 2024, Wiley-VCH [140]. (f) Chemical structure of the electrolyte components and ternary diagram of the prepared $Li_xH_yI_z$ ($x+y+z=1$) electrolyte, where x, y, and z correspond to the mole ratio of LiTFSI, H_2O, and IDE, respectively. The half-filled triangle denotes $Li_{0.1}H_{0.2}I_{0.7}$, the half-filled square denotes $Li_{0.2}H_{0.2}I_{0.6}$, the half-filled circle denotes $Li_{0.3}H_{0.2}I_{0.5}$, and the half-filled diamond denotes 21 M electrolyte. Reproduced with permission: Copyright 2024, Wiley-VCH [141].

reduce the desolvation energy barrier, form a wide electrochemical window, and exhibit excellent nonflammability and cycle stability (Figure 8c) [130, 144, 145]. Introducing polar protic solvents into aqueous electrolytes enhances the hydrogen-bond strength and is an economical means to suppress water activity. Polar protic solvents rearrange the network structure of water molecules through hydrogen bonding, thereby enabling close contact between the electrode and the electrolyte and suppressing proton coinsertion into the electrode during cycling. In diluted salt-solvent electrolytes, ions tend to dissolve in highly polar solvents (lower left in Figure 8d). Superconcentrated salts or "solvent-in-salt" will disrupt the intermolecular network in free solvent clusters (lower right in Figure 8d) [138]. Polar organic solvents as cosolvents can adjust the intermolecular hydrogen-bonding network. For example, ethylene glycol (EG) acts as an H-bond modulating agent and as a cosolvent, disrupts the hydrogen-bonding network in the diluted electrolyte to minimize HER (Figure 8e) [140]. Multiple oxygen atoms in the three-dimensional structure of the green cosolvent isosorbide dimethyl ether (IDE) regulate the intermolecular hydrogen-bonding network to restrict water molecules in the electrolyte (Figure 8f,g) [141].

As cosolvents, polar solvents can achieve the enhancement of diverse properties of aqueous electrolytes. For example, the polar organic solvent DMSO is an effective electrolyte additive. In zinc-ion batteries, dimethyl sulfoxide (DMSO), boasting a large Gutmann donor number, coordinates with Zn^{2+} ions before water molecules and replaces water in the solvation structure. The strong interaction between DMSO and water suppresses water activity and mitigates detrimental side reactions [146]. It has been found that no SEI is generated in this system during charging–discharging processes to impede side reactions and enhance the low-temperature performance. Therefore, the DMSO additive improves the low-temperature and electrochemical properties of the electrolyte (Figure 9a,b) [147]. By adding *N*,*N*-dimethylformamide (DMF) to the $Zn(CF_3SO_3)_2$–H_2O electrolyte, hydrogen bonding between DMF and H_2O inhibits the deprotonation of the electrolyte and restricts water molecules. As a result, the cycling lifespan and CE of the battery are improved (Figure 9d) [149].

In aqueous electrolytes, polar organic solvents enhance electrochemical polarization, decrease the surface energy of the electrode/electrolyte interface, form more active sites with smaller critical nucleus sizes and finer grains, and lead to stable interfacial chemistry. Adding the polar organic solvent polyethylene glycol (PEG) to the electrolyte enables Zn^{2+} to be deposited on the interface to form a smooth electrolyte/electrode interface, thereby avoiding the formation of dendrites and achieving stable interfacial deposition and electrochemical properties (Figure 9f and Figure S14) [150]. Wang and colleagues have added 0.05 M of $SnCl_2$ to the aqueous electrolyte to construct a double-layer SEI on the anode. The SEI consists of a zinc-phobic layer of $Zn_5(OH)_8Cl_2{\cdot}H_2O$ and a zincophilic layer that guides the uniform deposition of Zn^{2+} (Figure 9e) [118]. Yang and colleagues have formed a $Zn(ClO_4)_2$–succinonitrile (SN) aqueous solution eutectic electrolyte by forcing SN into the Zn solvation sheath to replace water molecules, reduce water decomposition, prevent the growth of Zn dendrites, and improve the CE of Zn plating/stripping (Figure 9c and Figure S15) [148].

Cosolvents can work synergistically with halogen ions to stabilize batteries. Polar organic solvent dimethyl carbonate (DMC) and halogen ion iodine (I_2) are electrolyte additives for

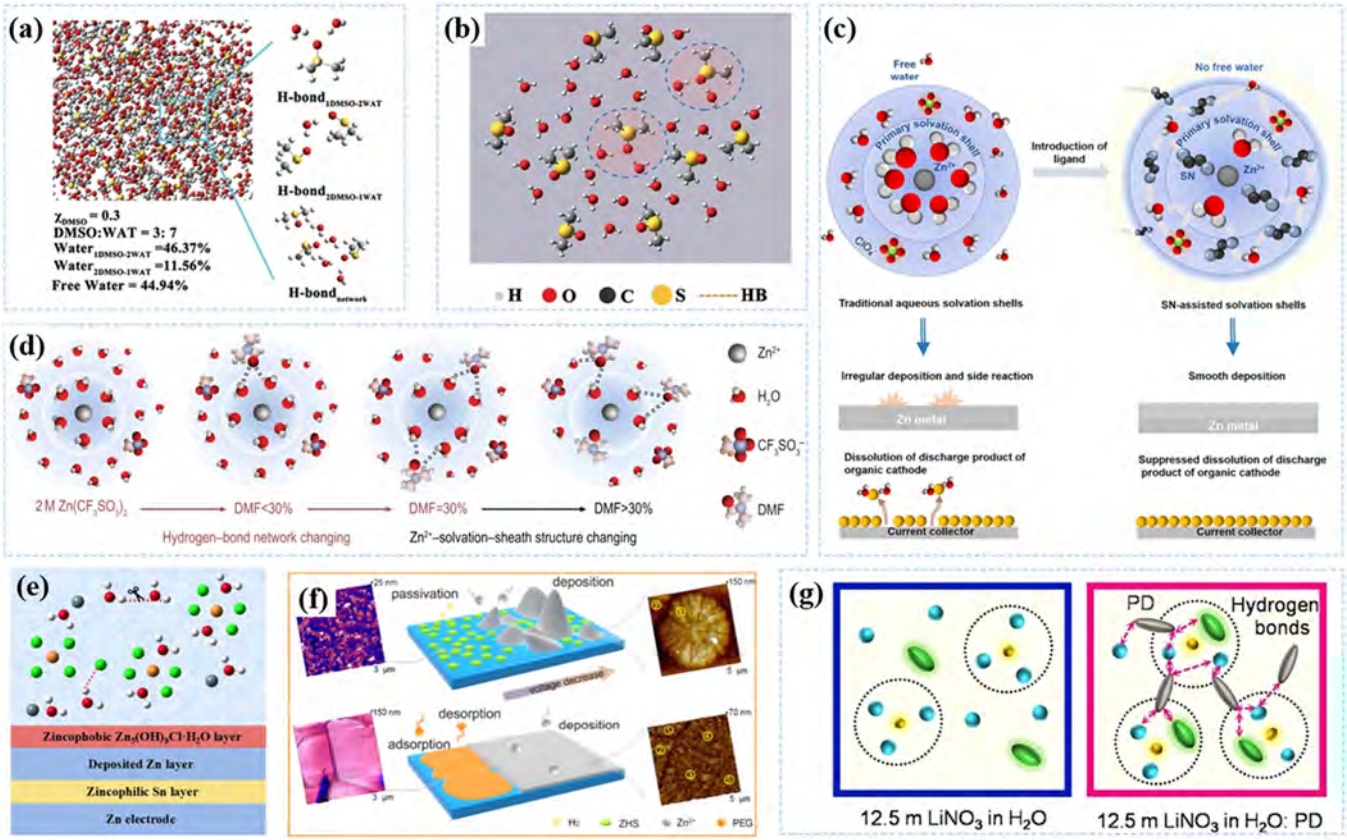

FIGURE 9 | Functions of polar solvents and halogen additives. (a) Conformation analysis of the system with $\chi_{DMSO} = 0.3$ from MD simulations. Reproduced with permission: Copyright 2019, Wiley-VCH [147]. (b) Local structure of the $\chi_{DMSO} = 0.3$ system from MD simulations. Reproduced with permission: Copyright 2019, Wiley-VCH [147]. (c) New hydrated eutectic electrolyte based on a simple formulation of a hydrated Zn salt and a neutral ligand. Reproduced with permission: Copyright 2020, Cell Press [148]. (d) Schematic of changes in Zn^{2+} solvent sheath and local hydrogen-bond network with DMF addition. Reproduced with permission: Copyright 2022, Oxford University Press [149]. (e) Schematic of the electrolyte and electrolyte–electrode interphase structure. (f) Mechanism of interfacial product evolution in 1.0 M $ZnSO_4$ and 1.0 M $ZnSO_4$–1000 ppm PEG electrolytes. The insets show enlarged voltage–time curves. Reproduced with permission: Copyright 2020, American Chemical Society [150]. (g) Corresponding hypothetical diagrams of solvation structures for the electrolytes. Reproduced with permission: Copyright 2021, Wiley-VCH [151].

the zinc trifluoromethanesulfonate ($Zn(OTf)_2$) solution. The addition of iodine (I_2) enhances the redox kinetics of the sulfur cathode, and the polar solvent DMC reduces the activity of free water. Molecular dynamics simulations show that polar organic solvents as additives can reduce the corrosion rate of zinc electrodes (Figure S16) [152], broaden the ESW, improve the wettability of the sulfur cathode, and stabilize the negative zinc electrode [153]. An aqueous hybrid electrolyte comprising dimethylacetamide (DMA) as a high-donor number organic co-solvent and ZnI_2 as an additive has been applied to high donor-number solvents to mitigate water-induced side reactions in other aqueous metal–sulfur batteries [154].

Both solvent additives and electrode additives can improve the performance of batteries to a certain extent, and the reasonable selection of additives is beneficial to the research of aqueous batteries. As a solvent additive different from cosolvents, inert diluents increase the ESW of electrolytes by forming locally concentrated WISEs. For example, 1,5-pentanediol (PD) as an inert diluent added to the WISE can maintain the solvation structure of the WIS electrolyte (Figure 9g). After cycling at 1 C 250 times, the average CE reaches 98.53% [151]. In recent years, the addition of nonionic surfactants has emerged as a novel electrolyte design concept, leveraging the self-assembly properties of surfactants to in situ form a liquid crystal interface phase (LCIP). This LCIP inhibits dendrite growth and side reactions through dynamic coordination and template growth mechanisms, providing a new direction for high-energy-density aqueous batteries [155]. Suo and colleagues have reported a bifunctional fluorine-containing electrode additive. Constructing a LiF-rich SEI layer and reducing battery polarization minimize the dependence of ALIBs on salts and high concentrations [156].

In distinct concentrated aqueous electrolyte systems, the formation mechanisms of SEI, regulations of solvation structures, and inhibitions of water activity exhibit notable discrepancies (Figure 10). Strongly solvated cations and polar solvents actively disrupt the inherent hydrogen-bonding networks among water molecules, then reconstruct new hydrogen bonds with water molecules. Cosolvent molecules competitively adsorb at the interface to displace water molecules, thereby reducing local water activity [157]. The introduction of multi-salt components and cosolvents breaks through the single "water-in-salt" concentration-dependent regulation, creating novel approaches for realizing lower water activity, broadened ESW, and sufficient interface stability [158].

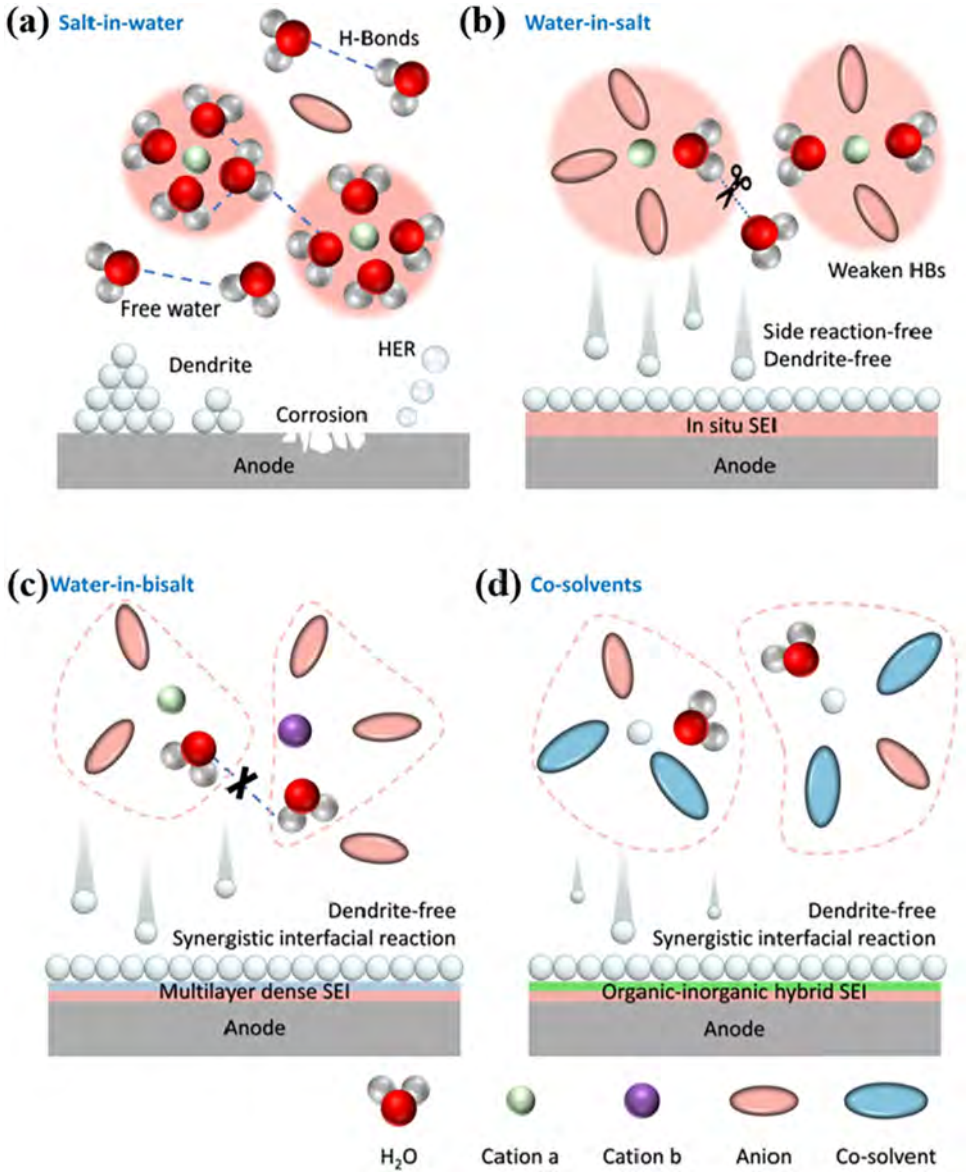

FIGURE 10 | Key mechanism schematic diagram. (a) Salt-in-water. (b) Water-in-salt. (c) Water-in-bisalt. (d) Cosolvents.

4 | Applications of High-Concentration Electrolytes

HCEs widen the ESW with WISE to address the most significant problem with aqueous batteries (Figure 11 and Table S2) [81, 89, 101, 102, 120, 133, 134, 137, 140]. Additionally, the disruption of the original hydrogen-bond network between water molecules and the reconstruction of hydrogen-bond networks are important strategies to broaden the temperature window of HCEs. Strategies such as increasing salt concentration to break hydrogen-bond networks, using functional additives and mixed salts to optimize solvation structures, employing gel electrolytes, and applying eutectic electrolytes have broadened the temperature range of aqueous batteries and achieved remarkable progress (Figure 12a) [159, 161]. The development history of high-concentration aqueous electrolytes is shown in Figure 12b [30, 94, 160].

HCEs offer a relatively wide ESW, high stability, and broad temperature adaptability, making their applications in rechargeable batteries, supercapacitors, and hybrid ion battery energy storage devices worthy of attention. In ALIBs, the wide electrochemical window of HCEs and the SEI membrane containing components like LiF contribute to the high energy density of full cells [162]. Additionally, they have been applied to sodium-ion, zinc-ion, and calcium-ion batteries [34, 163]. Flexible energy storage devices for wearables are becoming more popular [164]. However, the electrolytes used in most flexible batteries and supercapacitors contain strong acids, strong alkalis, or toxic and flammable organic solutions, which pose safety risks. HCE-based supercapacitors exhibit intrinsic safety and environmental friendliness. Additionally, the fluoride-free bisalt electrolyte incurs significantly lower costs than conventional organic electrolytes, holding critical significance for industrialization. With regard to supercapacitors, the lettuce coral-like structure of PEDOT-tos shows the widest ESW of PEDOT-tos supercapacitors in aqueous electrolytes [165]. Hybrid electrolytes can be prepared to enable HCE to withstand a low temperature and for fully printed flexible ARSIB [166, 167]. These batteries with various shapes can be used as energy wristbands for electronic watches in a bent state. Owing to the wide electrochemical

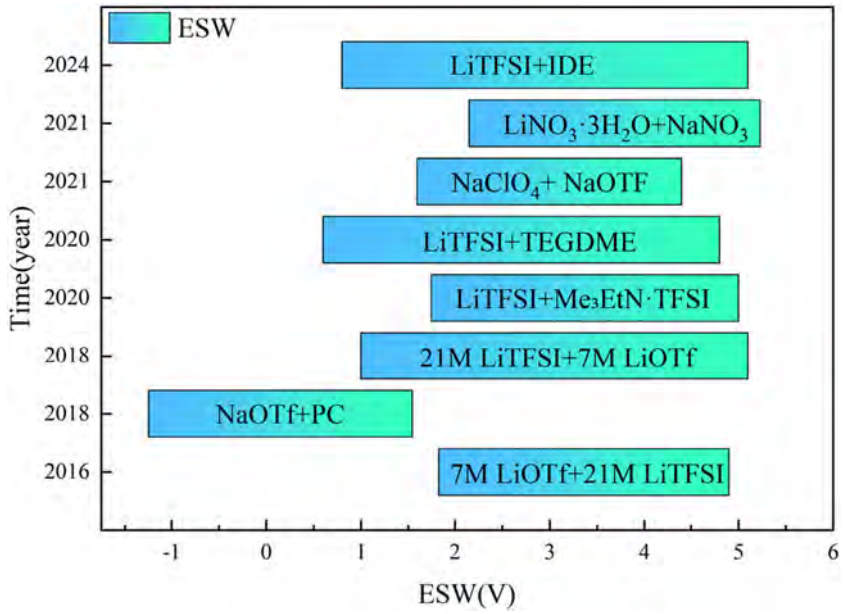

FIGURE 11 | Changes of ESW of different aqueous electrolytes [81, 89, 101, 102, 120, 133, 134, 137, 140].

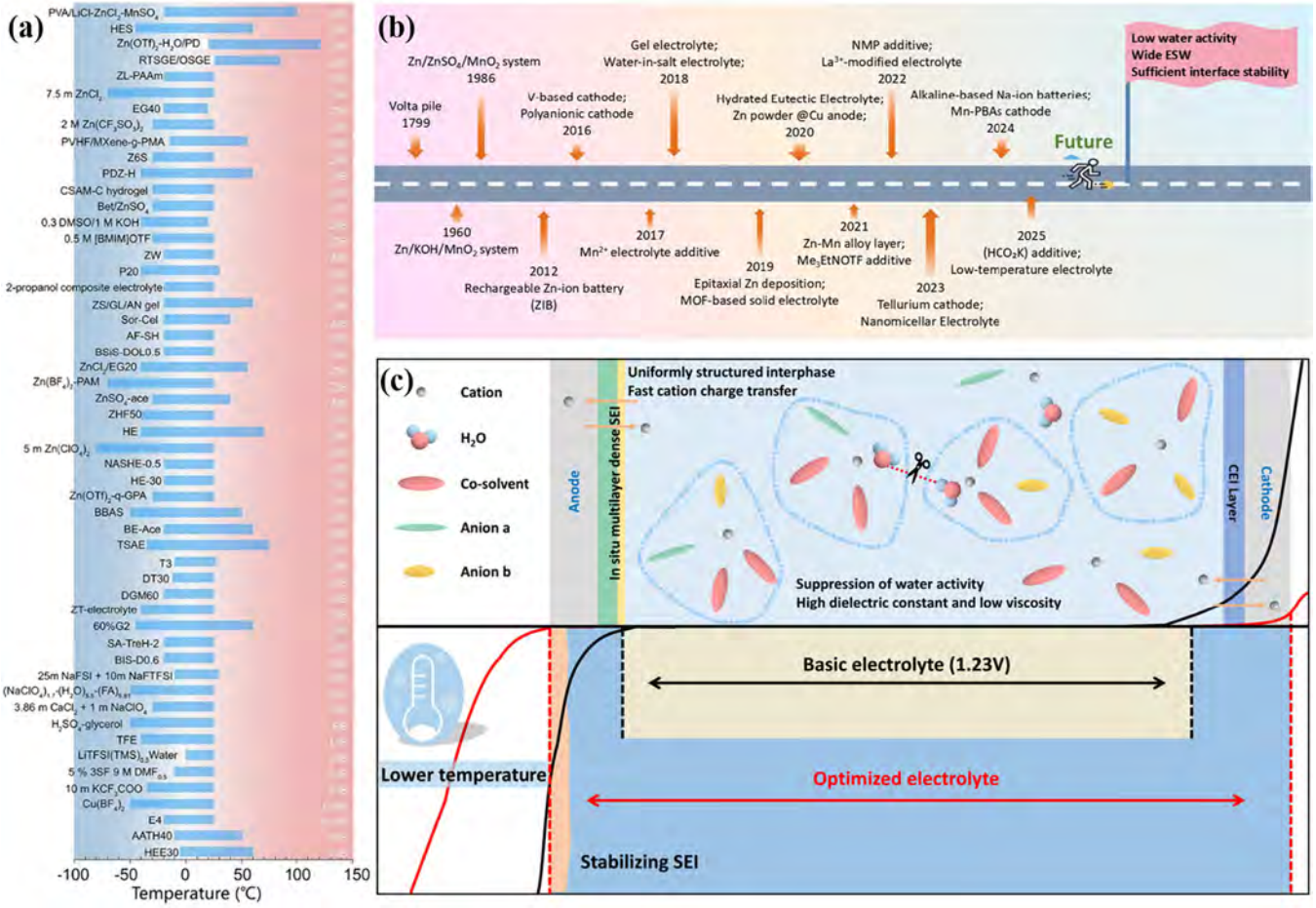

FIGURE 12 | Development of high-concentration electrolytes. (a) Research on operation under extreme temperatures. Reproduced with permission: Copyright 2025, *Energy & Environmental Science* [159]. (b) Development timeline of high-concentration electrolytes. Reproduced with permission: Copyright 2024, *Energy Storage Materials* [30, 94, 160]. (c) Future roadmap.

window and high energy density, HCE electrolytes are expected to be applicable to applications requiring high voltages and high energy densities, such as electric vehicles, large-scale EESs, and other devices [168, 169].

To accelerate the industrialization of HCEs in the future, electrolyte design should prioritize three key aspects: disrupting hydrogen-bond networks between water molecules, engineering artificial SEI interfaces, and achieving precise regulation of solvation structures (Figure 12c). The continuous increase in salt concentration in WIES imposes dual challenges of cost escalation and hindered ion migration, it is more effective to select solvent components with a high dielectric constant and low viscosity to achieve better performance [170]. The strategy of fluorine-free salts and solvent additives can alleviate the enormous cost pressure. Local concentrated electrolytes separate the bulk and interfacial properties of electrolytes by adding weakly polar polyfluorinated ethers as diluents, thereby reducing electrolyte concentration and cost (Figure S17 and Table S3) [12, 125, 147, 151].

5 | Summary and Outlook

WISEs are increasingly important and the modification strategies for high-concentration aqueous electrolyte systems are becoming diverse. This review summarizes the latest research activities and developments pertaining to electrolyte modification of aqueous batteries. The common strategies for HCEs regulation include WIS, WIBS electrolytes, multi-salt electrolytes, and solvent additives. Strongly solvated cationic salts can be one solution as they form dense and ordered solvation shells around them. Anions do not interact strongly with solvated cations and water molecules, thus creating a network that suppresses the activity of water molecules and participates in forming the solid-electrolyte interphase (SEI). Highly polar solvents are another factor. They promote the dissociation of salts to form fully solvated ions and stable complexes with metal ions. The molecular size and structure of these solvents affect the thickness of the solvation layer. Electrode materials with suitable structures and appropriate redox potentials can widen the ESW, form a complete SEI, improve conductivity, and inhibit the dissolution of electrode materials. The proper aqueous electrolytes are safe and have good electrochemical properties. The development of low-cost and wide-temperature-range electrolyte systems is pivotal for the future of aqueous electrolytes. Recent strategies leveraging machine learning and computational screening for electrolyte composition design offer novel pathways for rational development of large-scale energy storage batteries [171, 172]. However, further research is warranted in the following aspects:

1. Understanding water dynamics at the interface. As the core solvent in high-concentration aqueous electrolytes, clarifying the dynamic behavior and physicochemical processes of water molecules at the electrode/electrolyte interface is of great significance for the structural design of electrolytes
2. Enabling operation at extreme temperatures. The operation of aqueous electrolytes under extreme temperatures is a long-term and highly challenging issue. At low temperatures, the reduced movement speed of water molecules leads to hindered ion transport. At high temperatures, the increased activity of water molecules may cause the decomposition of the electrolyte and accelerate the corrosion of electrode materials and other problems. By optimizing the electrolyte, it is possible to achieve stable operation within a wider temperature range and broaden its application scenarios.
3. Standardizing performance metrics. At present, for the electrochemical performance tests of aqueous electrolytes, such as ionic conductivity and cycle life, there is a lack of standardized performance indicators, making it impossible to better evaluate the performance advantages and disadvantages of new electrolytes.

Author Contributions

Lingli Chen: writing – original draft (lead). **Yue Xu:** writing – original draft (lead); conceived and designed manuscript, supervision, funding acquisition. **Angran Liu:** writing – original draft (supporting). **Bo Cheng:** writing – original draft (supporting). **Sihan Wang:** writing – original draft (supporting). **Paul K. Chu:** writing – review and editing, conceived and designed manuscript, supervision, funding acquisition. **Yongbin Hua:** writing – review and editing. **Long Jiang:** writing – review and editing. **Xiaolin Zhang:** writing – review and editing. **Chun Fang:** conceived and designed manuscript, supervision, funding acquisition. **Jiantao Han:** conceived and designed manuscript, supervision, funding acquisition.

Acknowledgments

This work was supported by the National Natural Science Foundation of China (Nos. 22479057, 51902118), International Postdoctoral Exchange Fellowship Program (Grant No. PC2021026), Postdoctor Project of Hubei Province under Grant Number 2024HBBHXF083, and City University of Hong Kong Donation Research Grants (No. DON-RMG 9229021 and No. 9229021).

Conflicts of Interest

The authors declare no conflicts of interest.

References

1. H. Wang and H. Dai, "Strongly Coupled Inorganic–Nano-Carbon Hybrid Materials for Energy Storage," *Chemical Society Reviews* 42, no. 7 (2013): 3088.

2. X. Li, T. Zhang, G. Li, et al., "A Mn^{2+}-S Redox Electrochemistry for Energetic Aqueous Manganese Ion Battery," *Joule* 9, no. 6 (2025): 101930.

3. Z. Ju, Q. Zhao, D. Chao, et al., "Energetic Aqueous Batteries," *Advanced Energy Materials* 12, no. 27 (2022): 2201074.

4. Y. Lim, G. Lee, J. H. Kim, J. K. Seo, and S. J. Yoo, "Tetrabutylammonium Bromide Incorporated Hydrated Deep Eutectic Solvents: Simultaneously Addressing Anode Stability and Cathode Efficiency in Zinc-Bromine Batteries," *Energy Storage Materials* 68 (2024): 103331.

5. K. Zhang, L. Wang, C. Ma, et al., "A Comprehensive Evaluation of Battery Technologies for High–Energy Aqueous Batteries," *Small* 20, no. 13 (2024): 2309154.

6. H. Wang, S. Bi, Y. Zhang, J. Tian, and Z. Niu, "A High-Energy Aqueous All-Sulfur Battery," *Angewandte Chemie International Edition* 63, no. 10 (2024): e202317825.

7. M. Wang, Y. Meng, Y. Xu, et al., "Aqueous All-Manganese Batteries," *Energy & Environmental Science* 16, no. 11 (2023): 5284–5293.

8. R. Zhang, S. Wang, S. Chou, and H. Jin, "Research Development on Aqueous Ammonium-Ion Batteries," *Advanced Functional Materials* 32, no. 25 (2022): 2112179.

9. J. Han, A. Varzi, and S. Passerini, "The Emergence of Aqueous Ammonium-Ion Batteries," *Angewandte Chemie International Edition* 61, no. 14 (2022): e202115046.

10. H. Wang, Q. Wu, L. Cheng, and G. Zhu, "The Emerging Aqueous Zinc-Organic Battery," *Coordination Chemistry Reviews* 472 (2022): 214772.

11. Y. Dong, N. Zhang, Z. Wang, et al., "Cell-Nucleus Structured Electrolyte for Low-Temperature Aqueous Zinc Batteries," *Journal of Energy Chemistry* 83 (2023): 324–332.

12. L. Suo, O. Borodin, T. Gao, et al., "'Water-in-Salt' Electrolyte Enables High-Voltage Aqueous Lithium-Ion Chemistries," *Science* 350, no. 6263 (2015): 938–943.

13. Y. Miao, P. Yu, F. Yang, Y. Zhao, H. Xu, and J. Wang, "Effects of Cosolvent and Nonsolvating Solvent on the Structural Dynamics of Organic Electrolytes in Sodium-Ion Batteries," *ACS Applied Materials & Interfaces* 17, no. 1 (2025): 1064–1076.

14. B. Wu, Y. Mu, J. He, et al., "In Situ Characterizations for Aqueous Rechargeable Zinc Batteries," *Carbon Neutralization* 2, no. 3 (2023): 310–338.

15. J. Xu and C. Wang, "Perspective—Electrolyte Design for Aqueous Batteries: From Ultra-High Concentration to Low Concentration," *Journal of the Electrochemical Society* 169, no. 3 (2022): 030530.

16. D. Chao and S.-Z. Qiao, "Toward High-Voltage Aqueous Batteries: Super- or Low-Concentrated Electrolyte?," *Joule* 4, no. 9 (2020): 1846–1851.

17. G. A. Giffin, "The Role of Concentration in Electrolyte Solutions for Non-Aqueous Lithium-Based Batteries," *Nature Communications* 13, no. 1 (2022): 5250.

18. Y.-S. Hu and Y. Lu, "The Mystery of Electrolyte Concentration: From Superhigh to Ultralow," *ACS Energy Letters* 5, no. 11 (2020): 3633–3636.

19. M. Peng, L. Wang, L. Li, et al., "Molecular Crowding Agents Engineered to Make Bioinspired Electrolytes for High-Voltage Aqueous Supercapacitors," *eScience* 1, no. 1 (2021): 83–90.

20. J. Xie, Z. Liang, and Y.-C. Lu, "Molecular Crowding Electrolytes for High-Voltage Aqueous Batteries," *Nature Materials* 19, no. 9 (2020): 1006–1011.

21. Q. Dou, S. Lei, D.-W. Wang, et al., "Safe and High-Rate Supercapacitors Based on an "Acetonitrile/Water in Salt" Hybrid Electrolyte," *Energy & Environmental Science* 11, no. 11 (2018): 3212–3219.

22. L. Wang, H. Yu, D. Chen, et al., "Steric Hindrance and Orientation Polarization by a Zwitterionic Additive to Stabilize Zinc Metal Anodes," *Carbon Neutralization* 3, no. 6 (2024): 996–1008.

23. K. Zhu, Z. Li, Z. Sun, et al., "Inorganic Electrolyte for Low-Temperature Aqueous Sodium Ion Batteries," *Small* 18, no. 14 (2022): 2107662.

24. J. Chen, W. Zhou, Y. Quan, et al., "Ionic Liquid Additive Enabling Anti-Freezing Aqueous Electrolyte and Dendrite-Free Zn Metal Electrode With Organic/Inorganic Hybrid Solid Electrolyte Interphase Layer," *Energy Storage Materials* 53 (2022): 629–637.

25. Z. Tian, J. Yin, T. Guo, et al., "A Sustainable NH_4^+ Ion Battery by Electrolyte Engineering," *Angewandte Chemie* 134, no. 51 (2022): e202213757.

26. C. Sun, C. Wu, X. Gu, C. Wang, and Q. Wang, "Interface Engineering via $Ti_3C_2T_x$ MXene Electrolyte Additive Toward Dendrite-Free Zinc Deposition," *Nano-Micro Letters* 13, no. 1 (2021): 89.

27. W. Li, J. R. Dahn, and D. S. Wainwright, "Rechargeable Lithium Batteries With Aqueous Electrolytes," *Science* 264, no. 5162 (1994): 1115–1118.

28. Y. Shen, B. Liu, X. Liu, et al., "Water-in-Salt Electrolyte for Safe and High-Energy Aqueous Battery," *Energy Storage Materials* 34 (2021): 461–474.

29. T. Schuler, T. Kimura, T. J. Schmidt, and F. N. Büchi, "Towards a Generic Understanding of Oxygen Evolution Reaction Kinetics in Polymer Electrolyte Water Electrolysis," *Energy & Environmental Science* 13, no. 7 (2020): 2153–2166.

30. H. Wu, J. Hao, Y. Jiang, et al., "Alkaline-Based Aqueous Sodium-Ion Batteries for Large-Scale Energy Storage," *Nature Communications* 15, no. 1 (2024): 575.

31. D. Xiao, L. Zhang, Z. Li, H. Dou, and X. Zhang, "Design Strategies and Research Progress for Water-in-Salt Electrolytes," *Energy Storage Materials* 44 (2022): 10–28.

32. Y. Xu, X. Zhou, Z. Chen, Y. Hou, Y. You, and J. Lu, "Electrolyte Formulas of Aqueous Zinc Ion Battery: A Physical Difference With Chemical Consequences," *Materials Today* 66 (2023): 339–347.

33. C.-H. Lin, L. Wang, S. T. King, et al., "Probing Kinetics of Water-in-Salt Aqueous Batteries With Thick Porous Electrodes," *ACS Central Science* 7, no. 10 (2021): 1676–1687.

34. J. Zhao, Y. Li, X. Peng, et al., "High-Voltage Zn/$LiMn_{0.8}Fe_{0.2}PO_4$ Aqueous Rechargeable Battery by Virtue of "Water-in-Salt" Electrolyte," *Electrochemistry Communications* 69 (2016): 6–10.

35. S. Liu, R. Zhang, J. Mao, et al., "Design of Electrolyte for Boosted Aqueous Battery Performance: A Critical Review and Perspective," *Applied Physics Reviews* 10, no. 2 (2023): 021304.

36. J. Han, M. Zarrabeitia, A. Mariani, et al., "Concentrated Electrolytes Enabling Stable Aqueous Ammonium-Ion Batteries," *Advanced Materials* 34, no. 32 (2022): 2201877.

37. K. Qian, Z. Yu, Y. Liu, et al., "Understanding Fluorine-Free Electrolytes via Small-Angle X-Ray Scattering," *Journal of Energy Chemistry* 70 (2022): 340–346.

38. T. Liang, R. Hou, Q. Dou, H. Zhang, and X. Yan, "The Applications of Water-in-Salt Electrolytes in Electrochemical Energy Storage Devices," *Advanced Functional Materials* 31, no. 3 (2021): 2006749.

39. X. Liu, S.-C. Lee, S. Seifer, et al., "Insight into the Nanostructure of 'Water in Salt' Solutions: A SAXS/WAXS Study on Imide-Based Lithium Salts Aqueous Solutions," *Energy Storage Materials* 45 (2022): 696–703.

40. C. Zhong, B. Liu, J. Ding, et al., "Decoupling Electrolytes Towards Stable and High-Energy Rechargeable Aqueous Zinc–Manganese Dioxide Batteries," *Nature Energy* 5, no. 6 (2020): 440–449.

41. Y. Zhu, Y. Cui, Z. Xie, Z. Zhuang, G. Huang, and X. Zhang, "Decoupled Aqueous Batteries Using pH-Decoupling Electrolytes," *Nature Reviews Chemistry* 6, no. 7 (2022): 505–517.

42. Y. Sui and X. Ji, "Electrolyte Interphases in Aqueous Batteries," *Angewandte Chemie International Edition* 63, no. 2 (2024): e202312585.

43. Q. Dong, X. Yao, Y. Zhao, et al., "Cathodically Stable Li-O_2 Battery Operations Using Water-in-Salt Electrolyte," *Chem* 4, no. 6 (2018): 1345–1358.

44. H. Zhang, S. Jeong, B. Qin, D. Vieira Carvalho, D. Buchholz, and S. Passerini, "Towards High-Performance Aqueous Sodium-Ion Batteries: Stabilizing the Solid/Liquid Interface for NASICON-Type $Na_2VTi(PO_4)_3$ Using Concentrated Electrolytes," *ChemSusChem* 11, no. 8 (2018): 1382–1389.

45. R.-S. Kühnel, D. Reber, and C. Battaglia, "A High-Voltage Aqueous Electrolyte for Sodium-Ion Batteries," *ACS Energy Letters* 2, no. 9 (2017): 2005–2006.

46. L. Jiang, Y. Lu, C. Zhao, et al., "Building Aqueous K-Ion Batteries for Energy Storage," *Nature Energy* 4, no. 6 (2019): 495–503.

47. Z. Li, D. Young, K. Xiang, W. C. Carter, and Y. M. Chiang, "Towards High Power High Energy Aqueous Sodium-Ion Batteries: The

$NaTi_2(PO_4)_3/Na_{0.44}MnO_2$ System," *Advanced Energy Materials* 3, no. 3 (2013): 290–294.

48. M. Kumar, A. K. Padhan, D. Mandal, and T. C. Nagaiah, "An Elemental Sulfur/CoS_{2-} Ionic Liquid Based Anode for High-Performance Aqueous Sodium-Ion Batteries," *Energy Storage Materials* 45 (2022): 1052–1061.

49. Q. Wang, C. Wang, Y. Qiao, H. Zhou, and J. Yu, "Hybrid-Electrolytes System Established by Dual Super-Lyophobic Membrane Enabling High-Voltage Aqueous Lithium Metal Batteries," *Advanced Materials* 36, no. 26 (2024): 2401486.

50. O. Borodin, J. Self, K. A. Persson, C. Wang, and K. Xu, "Uncharted Waters: Super-Concentrated Electrolytes," *Joule* 4, no. 1 (2020): 69–100.

51. X. Li, X. Wang, L. Ma, and W. Huang, "Solvation Structures in Aqueous Metal-Ion Batteries," *Advanced Energy Materials* 12, no. 37 (2022): 2202068.

52. Z. Khan, D. Kumar, and X. Crispin, "Does Water-in-Salt Electrolyte Subdue Issues of Zn Batteries?," *Advanced Materials* 35, no. 36 (2023): 2300369.

53. P. Yi, Z. Li, L. Ma, et al., "Eco-Friendly High-Performance Symmetric All-COF/Graphene Aqueous Zinc-Ion Batteries," *Advanced Materials* 36 (2024): 2414379.

54. Y. Feng, X. Yu, B. Wang, et al., "Thiosulfate-Mediated Polysulfide Redox for Energetic Aqueous Battery," *Angewandte Chemie International Edition* 64 (2024): e202420514.

55. D. P. Leonard, Z. Wei, G. Chen, F. Du, and X. Ji, "Water-in-Salt Electrolyte for Potassium-Ion Batteries," *ACS Energy Letters* 3, no. 2 (2018): 373–374.

56. Y. Zhu, H. Y. Hoh, S. Qian, et al., "Ultrastable Zinc Anode Enabled by CO_2-Induced Interface Layer," *ACS Nano* 16, no. 9 (2022): 14600–14610.

57. Q. Y. Meng, J. C. Shao, X. R. Dou, and H. Z. Chi, "N-Containing $Na_2VTi(PO_4)_3$/C for Aqueous Sodium-Ion Batteries," *Small* 20, no. 28 (2024): 2308483.

58. B. Zhao, Q. Wang, S. Zhang, and C. Deng, "Self-Assembled Wafer-Like Porous $NaTi_2(PO_4)_3$ Decorated With Hierarchical Carbon as a High-Rate Anode for Aqueous Rechargeable Sodium Batteries," *Journal of Materials Chemistry A* 3, no. 22 (2015): 12089–12096.

59. X. Wu, M. Sun, Y. Shen, et al., "Energetic Aqueous Rechargeable Sodium-Ion Battery Based on $Na_2CuFe(CN)_6$–$NaTi_2(PO_4)_3$ Intercalation Chemistry," *ChemSusChem* 7, no. 2 (2014): 407–411.

60. C. Yang, L. Suo, O. Borodin, et al., "Unique Aqueous Li-Ion/Sulfur Chemistry With High Energy Density and Reversibility," *Proceedings of the National Academy of Sciences* 114, no. 24 (2017): 6197–6202.

61. X. Li, Y. Shen, D. Kong, et al., "Realizing an Aqueous Sodium-Ion Battery With a Super-High Discharge Voltage Based on a Novel FeSe$_2$@rGO Anode," *Inorganic Chemistry Frontiers* 9, no. 8 (2022): 1622–1629.

62. M. Kumar, N. Thakur, A. Bordoloi, et al., "High-Performance Aqueous Sodium-Ion/Sulfur Battery Using Elemental Sulfur," *Journal of Materials Chemistry A* 10, no. 21 (2022): 11394–11404.

63. X. Tang, D. Zhou, B. Zhang, et al., "A Universal Strategy Towards High–Energy Aqueous Multivalent–Ion Batteries," *Nature Communications* 12, no. 1 (2021): 2857.

64. C. Liu, X. Xie, B. Lu, J. Zhou, and S. Liang, "Electrolyte Strategies Toward Better Zinc-Ion Batteries," *ACS Energy Letters* 6, no. 3 (2021): 1015–1033.

65. Y. Du, Y. Li, B. B. Xu, et al., "Electrolyte Salts and Additives Regulation Enables High Performance Aqueous Zinc Ion Batteries: A Mini Review," *Small* 18, no. 43 (2022): 2104640.

66. M. Zhu, X. Wang, H. Tang, et al., "Antifreezing Hydrogel With High Zinc Reversibility for Flexible and Durable Aqueous Batteries by Cooperative Hydrated Cations," *Advanced Functional Materials* 30, no. 6 (2020): 1907218.

67. Y. Jin, K. S. Han, Y. Shao, et al., "Stabilizing Zinc Anode Reactions by Polyethylene Oxide Polymer in Mild Aqueous Electrolytes," *Advanced Functional Materials* 30, no. 43 (2020): 2003932.

68. Y. Yang, Z. Bai, S. Liu, et al., "Self-Protecting Aqueous Lithium-Ion Batteries," *Small* 18, no. 38 (2022): 2203035.

69. Y. Liu, Y. Qiao, X. Lou, X. Zhang, W. Zhang, and Y. Huang, "Hollow $K_{0.27}MnO_2$ Nanospheres as Cathode for High-Performance Aqueous Sodium Ion Batteries," *ACS Applied Materials & Interfaces* 8, no. 23 (2016): 14564–14571.

70. Z. Hou, X. Li, J. Liang, Y. Zhu, and Y. Qian, "An Aqueous Rechargeable Sodium Ion Battery Based on a $NaMnO_2$–$NaTi_2(PO_4)_3$ Hybrid System for Stationary Energy Storage," *Journal of Materials Chemistry A* 3, no. 4 (2015): 1400–1404.

71. C. W. Mason and F. Lange, "Aqueous Ion Battery Systems Using Sodium Vanadium Phosphate Stabilized by Titanium Substitution," *ECS Electrochemistry Letters* 4, no. 8 (2015): A79–A82.

72. T. Gu, M. Zhou, M. Liu, K. Wang, S. Cheng, and K. Jiang, "A Polyimide–MWCNTs Composite as High Performance Anode for Aqueous Na-Ion Batteries," *RSC Advances* 6, no. 58 (2016): 53319–53323.

73. X. Wu, Y. Cao, X. Ai, J. Qian, and H. Yang, "A Low-Cost and Environmentally Benign Aqueous Rechargeable Sodium-Ion Battery Based on $NaTi_2(PO_4)_3$–$Na_2NiFe(CN)_6$ Intercalation Chemistry," *Electrochemistry Communications* 31 (2013): 145–148.

74. L. Jiang, L. Liu, J. Yue, et al., "High-Voltage Aqueous Na-Ion Battery Enabled by Inert-Cation-Assisted Water-in-Salt Electrolyte," *Advanced Materials* 32, no. 2 (2020): 1904427.

75. X. Wu, Y. Xu, C. Zhang, et al., "Reverse Dual-Ion Battery via a $ZnCl_2$ Water-in-Salt Electrolyte," *Journal of the American Chemical Society* 141, no. 15 (2019): 6338–6344.

76. S. Li, Z. Zhang, J. Wu, et al., "Stable Zn–WO_3 Battery With a $ZnCl_2$ Water-in-Salt Electrolyte," *Journal of Power Sources* 560 (2023): 232691.

77. D. Kumar, L. R. Franco, N. Abdou, et al., "Water-in-Polymer Salt Electrolyte for Long-Life Rechargeable Aqueous Zinc-Lignin Battery," *Energy & Environmental Materials* 8 (2024): e12752.

78. N. Zhang, B. Wang, F. Jin, et al., "Modified Cathode-Electrolyte Interphase Toward High-Performance Batteries," *Cell Reports Physical Science* 3, no. 12 (2022): 101197.

79. Z. Yao, W. Zhang, and J. Zhu, "Stabilization of Cathode Electrolyte Interphase for Aqueous Zinc-Ion Batteries," *Journal of Energy Chemistry* 96 (2024): 359–386.

80. Q. Zhang, X. Liu, Y. Lu, et al., "Sustainable Aqueous Batteries Based on Bipolar Dissociation of Aluminum Hydroxyacetate Electrolyte," *Journal of the American Chemical Society* 146, no. 8 (2024): 5597–5604.

81. Q. Yang, W. Wang, H. Li, J. Zhang, F. Kang, and B. Li, "Investigation of Iron Hexacyanoferrate as a High Rate Cathode for Aqueous Batteries: Sodium-Ion Batteries and Lithium-Ion Batteries," *Electrochimica Acta* 270 (2018): 96–103.

82. H. Zhang, T. Xia, R. Chen, et al., "Confined Water Dynamics in Topological Networks Hydrogel for Aqueous Electrochemical Devices," *Small* 21 (2024): 2408819.

83. L. Zhong, Y. Lu, H. Li, Z. Tao, and J. Chen, "High-Performance Aqueous Sodium-Ion Batteries With Hydrogel Electrolyte and Alloxazine/CMK-3 Anode," *ACS Sustainable Chemistry & Engineering* 6, no. 6 (2018): 7761–7768.

84. M. Zhou, Y. Chen, G. Fang, and S. Liang, "Electrolyte/Electrode Interfacial Electrochemical Behaviors and Optimization Strategies in Aqueous Zinc-Ion Batteries," *Energy Storage Materials* 45 (2022): 618–646.

85. L. Miao, R. Wang, S. Di, et al., "Aqueous Electrolytes With Hydrophobic Organic Cosolvents for Stabilizing Zinc Metal Anodes," *ACS Nano* 16, no. 6 (2022): 9667–9678.

86. Z. Liu, R. Wang, Q. Ma, et al., "Application of Cellulose-Based Hydrogel Electrolytes in Flexible Batteries," *Carbon Neutralization* 1, no. 2 (2022): 126–139.

87. L. Sun, Y. Yao, L. Dai, et al., "Sustainable and High-Performance Zn Dual-Ion Batteries With a Hydrogel-Based Water-in-Salt Electrolyte," *Energy Storage Materials* 47 (2022): 187–194.

88. X. Chi, M. Li, X. Chen, et al., "Enabling High-Performance All-Solid-State Batteries via Guest Wrench in Zeolite Strategy," *Journal of the American Chemical Society* 145, no. 44 (2023): 24116–24125.

89. L. Suo, O. Borodin, W. Sun, et al., "Advanced High-Voltage Aqueous Lithium-Ion Battery Enabled by "Water-in-Bisalt" Electrolyte," *Angewandte Chemie International Edition* 55, no. 25 (2016): 7136–7141.

90. D. Dong, C. Zhao, X. Zhang, and C. Wang, "From Salt in Water, Water in Salt to Beyond," *Advanced Materials* (2025): 2418700.

91. S. Liu, J. Mao, W. K. Pang, et al., "Tuning the Electrolyte Solvation Structure to Suppress Cathode Dissolution, Water Reactivity, and Zn Dendrite Growth in Zinc-Ion Batteries," *Advanced Functional Materials* 31, no. 38 (2021): 2104281.

92. L. Lei, Y. Sun, X. Wang, Y. Jiang, and J. Li, "Strategies to Enhance Corrosion Resistance of Zn Electrodes for Next Generation Batteries," *Frontiers in Materials* 7 (2020): 96.

93. Y. Liang, M. Qiu, P. Sun, and W. Mai, "Comprehensive Review of Electrolyte Modification Strategies for Stabilizing Zn Metal Anodes," *Advanced Functional Materials* 33, no. 51 (2023): 2304878.

94. H. Ren, S. Li, B. Wang, et al., "Mapping the Design of Electrolyte Additive for Stabilizing Zinc Anode in Aqueous Zinc Ion Batteries," *Energy Storage Materials* 68 (2024): 103364.

95. P. Zou, C. Wang, Y. He, H. L. Xin, and R. Lin, "A Water-in-Salt Electrolyte for Room-Temperature Fluoride-Ion Batteries Based on a Hydrophobic–Hydrophilic Salt," *Nano Letters* 24, no. 18 (2024): 5429–5435.

96. W. Yuan, G. Ma, X. Nie, et al., "In-Situ Construction of a Hydroxide-Based Solid Electrolyte Interphase for Robust Zinc Anodes," *Chemical Engineering Journal* 431 (2022): 134076.

97. W. Tang, L. Deng, L. Guo, S. Zhou, Q. Jiang, and J. Luo, "Reversible Aqueous Aluminum Metal Batteries Enabled by a Water-in-Salt Electrolyte," *Green Energy & Environment* 9, no. 7 (2024): 1183–1191.

98. X. Zeng, J. Mao, J. Hao, et al., "Electrolyte Design for In Situ Construction of Highly Zn^{2+}-Conductive Solid Electrolyte Interphase to Enable High-Performance Aqueous Zn-Ion Batteries Under Practical Conditions," *Advanced Materials* 33, no. 11 (2021): 2007416.

99. F. Wan, X. Zhou, Y. Lu, Z. Niu, and J. Chen, "Energy Storage Chemistry in Aqueous Zinc Metal Batteries," *ACS Energy Letters* 5, no. 11 (2020): 3569–3590.

100. D. Li, L. Cao, T. Deng, S. Liu, and C. Wang, "Design of a Solid Electrolyte Interphase for Aqueous Zn Batteries," *Angewandte Chemie International Edition* 60, no. 23 (2021): 13035–13041.

101. T. Jin, X. Ji, P. F. Wang, et al., "High-Energy Aqueous Sodium-Ion Batteries," *Angewandte Chemie International Edition* 60, no. 21 (2021): 11943–11948.

102. L. Chen, J. Zhang, Q. Li, et al., "A 63 *m* Superconcentrated Aqueous Electrolyte for High-Energy Li-Ion Batteries," *ACS Energy Letters* 5, no. 3 (2020): 968–974.

103. M. Becker, D. Rentsch, D. Reber, A. Aribia, C. Battaglia, and R. S. Kühnel, "The Hydrotropic Effect of Ionic Liquids in Water-in-Salt Electrolytes," *Angewandte Chemie International Edition* 60, no. 25 (2021): 14100–14108.

104. Y. An, Y. Tian, K. Zhang, et al., "Stable Aqueous Anode-Free Zinc Batteries Enabled by Interfacial Engineering," *Advanced Functional Materials* 31, no. 26 (2021): 2101886.

105. L. Ma, T. P. Pollard, Y. Zhang, et al., "Ammonium Enables Reversible Aqueous Zn Battery Chemistries by Tailoring the Interphase," *One Earth* 5, no. 4 (2022): 413–421.

106. L. Cao, D. Li, T. Pollard, et al., "Fluorinated Interphase Enables Reversible Aqueous Zinc Battery Chemistries," *Nature Nanotechnology* 16, no. 8 (2021): 902–910.

107. L. Qian, H. Zhu, T. Qin, et al., "Ultralow-Salt-Concentration Electrolyte for High-Voltage Aqueous Zn Metal Batteries," *Advanced Functional Materials* 33, no. 23 (2023): 2301118.

108. J. Xu, X. Ji, J. Zhang, et al., "Aqueous Electrolyte Design for Super-Stable 2.5 V $LiMn_2O_4||Li_4Ti_5O_{12}$ Pouch Cells," *Nature Energy* 7, no. 2 (2022): 186–193.

109. Z. Zhao, J. Lai, D. T. Ho, et al., "A Novel "Water-in-Ionic Liquid" Electrolyte for Zn Metal Batteries," *ACS Energy Letters* 8, no. 1 (2023): 608–618.

110. C. Zhang, L. Zhang, and G. Yu, "Eutectic Electrolytes as a Promising Platform for Next-Generation Electrochemical Energy Storage," *Accounts of Chemical Research* 53, no. 8 (2020): 1648–1659.

111. J. Wu, Q. Liang, X. Yu, et al., "Deep Eutectic Solvents for Boosting Electrochemical Energy Storage and Conversion: A Review and Perspective," *Advanced Functional Materials* 31, no. 22 (2021): 2011102.

112. H. Qiu, X. Du, J. Zhao, et al., "Zinc Anode-Compatible In-Situ Solid Electrolyte Interphase via Cation Solvation Modulation," *Nature Communications* 10, no. 1 (2019): 5374.

113. J. Zhao, J. Zhang, W. Yang, et al., "Water-in-Deep Eutectic Solvent" Electrolytes Enable Zinc Metal Anodes for Rechargeable Aqueous Batteries," *Nano Energy* 57 (2019): 625–634.

114. P. Jiang, L. Chen, H. Shao, et al., "Methylsulfonylmethane-Based Deep Eutectic Solvent as a New Type of Green Electrolyte for a High-Energy-Density Aqueous Lithium-Ion Battery," *ACS Energy Letters* 4, no. 6 (2019): 1419–1426.

115. J. Wei, P. Zhang, J. Sun, et al., "Advanced Electrolytes for High-Performance Aqueous Zinc-Ion Batteries," *Chemical Society Reviews* 53, no. 20 (2024): 10335–10369.

116. Y. Zhu, J. Yin, X. Zheng, et al., "Concentrated Dual-Cation Electrolyte Strategy for Aqueous Zinc-Ion Batteries," *Energy & Environmental Science* 14, no. 8 (2021): 4463–4473.

117. Q. Zhang, Y. Ma, Y. Lu, et al., "Designing Anion-Type Water-Free Zn^{2+} Solvation Structure for Robust Zn Metal Anode," *Angewandte Chemie International Edition* 60, no. 43 (2021): 23357–23364.

118. L. Cao, D. Li, F. A. Soto, et al., "Highly Reversible Aqueous Zinc Batteries Enabled by Zincophilic–Zincophobic Interfacial Layers and Interrupted Hydrogen-Bond Electrolytes," *Angewandte Chemie International Edition* 60, no. 34 (2021): 18845–18851.

119. Y. Yu, J. Xu, K. Duanmu, et al., "Stabilizing Graphite Anode in Electrolytes With Nanoscale Anion Networking for High-Rate Lithium Storage," *ACS Energy Letters* 9, no. 10 (2024): 5002–5011.

120. Z. Wang, Y. Xu, J. Peng, et al., "A High Rate and Stable Hybrid Li/Na-Ion Battery Based on a Hydrated Molten Inorganic Salt Electrolyte," *Small* 17, no. 40 (2021): 2101650.

121. P. Wang, X. Xie, Z. Xing, et al., "Mechanistic Insights of Mg^{2+}-Electrolyte Additive for High-Energy and Long-Life Zinc-Ion Hybrid Capacitors," *Advanced Energy Materials* 11, no. 30 (2021): 21011 58.

122. A. Bayaguud, X. Luo, Y. Fu, and C. Zhu, "Cationic Surfactant-Type Electrolyte Additive Enables Three-Dimensional Dendrite-Free Zinc Anode for Stable Zinc-Ion Batteries," *ACS Energy Letters* 5, no. 9 (2020): 3012–3020.

123. J. Zhang, C. Cui, P.-F. Wang, et al., "'Water-in-Salt' Polymer Electrolyte for Li-Ion Batteries," *Energy & Environmental Science* 13, no. 9 (2020): 2878–2887.

124. Q. Zhang, Y. Ma, Y. Lu, et al., "Halogenated Zn^{2+} Solvation Structure for Reversible Zn Metal Batteries," *Journal of the American Chemical Society* 144, no. 40 (2022): 18435–18443.

125. W. Deng, X. Wang, C. Liu, et al., "Li/K Mixed Superconcentrated Aqueous Electrolyte Enables High-Performance Hybrid Aqueous Supercapacitors," *Energy Storage Materials* 20 (2019): 373–379.

126. J. Han, M. Zarrabeitia, A. Mariani, et al., "Halide-Free Water-in-Salt Electrolytes for Stable Aqueous Sodium-Ion Batteries," *Nano Energy* 77 (2020): 105176.

127. S. Liu, J. Xia, W. Zhang, et al., "Salt-in-Salt Reinforced Carbonate Electrolyte for Li Metal Batteries," *Angewandte Chemie International Edition* 61, no. 43 (2022): e202210522.

128. C. Zhu, L. Yan, Y. Han, et al., "Synergistic Modulation of Alkaline Aluminum-Air Battery Based on Localized Water-in-Salt Electrolyte Towards Anodic Self-Corrosion," *Chemical Engineering Journal* 485 (2024): 149600.

129. K. B. Ludwig, R. Correll-Brown, M. Freidlin, et al., "Highly Conductive Polyacrylonitrile-Based Hybrid Aqueous/Ionic Liquid Solid Polymer Electrolytes With Tunable Passivation for Li-Ion Batteries," *Electrochimica Acta* 453 (2023): 142349.

130. R. Chua, Y. Cai, P. Q. Lim, et al., "Hydrogen-Bonding Interactions in Hybrid Aqueous/Nonaqueous Electrolytes Enable Low-Cost and Long-Lifespan Sodium-Ion Storage," *ACS Applied Materials & Interfaces* 12, no. 20 (2020): 22862–22872.

131. C. Li, X. Jiang, H. Qi, et al., "Interfacial Dual-Modulation Through Deoxygenation Effect and Tuning Hydrogen-Bonding Environment Toward Highly Reversible Zn Metal Anodes," *Energy Storage Materials* 75 (2025): 104012.

132. T.-W. Lin, M. S. Kumar, H.-H. Shen, and J.-Y. Lin, "Acetamide-Based Deep Eutectic Solvents as Efficient Electrolytes for K–MnHCFe//Zn Dual-ion Batteries," *Journal of Power Sources* 614 (2024): 234972.

133. H. Zhang, B. Qin, J. Han, and S. Passerini, "Aqueous/Nonaqueous Hybrid Electrolyte for Sodium-Ion Batteries," *ACS Energy Letters* 3, no. 7 (2018): 1769–1770.

134. F. Wang, O. Borodin, M. S. Ding, et al., "Hybrid Aqueous/Non-Aqueous Electrolyte for Safe and High-Energy Li-Ion Batteries," *Joule* 2, no. 5 (2018): 927–937.

135. H. Lohani, A. Kumar, A. Bano, et al., "Inclusion of Anion Additives in the Inner Solvation Shell to Regulate the Composition of Solid Electrolyte Interphase," *Advanced Energy Materials* 14, no. 32 (2024): 2401268.

136. R. K. Gautam, J. J. McGrath, X. Wang, and J. J. Jiang, "Air-Stable Membrane-Free Magnesium Redox Flow Batteries," *Journal of the American Chemical Society* 146 (2024): jacs.4c10106.

137. J. Zhu, Y. Xu, Y. Fu, et al., "Hybrid Aqueous/Nonaqueous Water-in-Bisalt Electrolyte Enables Safe Dual Ion Batteries," *Small* 16, no. 17 (2020): 1905838.

138. C. Yang, J. Xia, C. Cui, et al., "All-Temperature Zinc Batteries With High-Entropy Aqueous Electrolyte," *Nature Sustainability* 6, no. 3 (2023): 325–335.

139. M. Kumar and T. C. Nagaiah, "Tuning the Interfacial Chemistry for Stable and High Energy Density Aqueous Sodium-Ion/Sulfur Batteries," *Journal of Materials Chemistry A* 10, no. 24 (2022): 12984–12996.

140. H. Fei, F. Yang, Z. Jusys, S. Passerini, and A. Varzi, "Ethylene Glycol Co-Solvent Enables Stable Aqueous Ammonium-Ion Batteries With Diluted Electrolyte," *Advanced Functional Materials* 34 (2024): 2404560.

141. Y. Wang, T. Ou, Y. Dong, et al., "A Green Asymmetric Bicyclic Co-Solvent Molecule for High-Voltage Aqueous Lithium-Ion Batteries," *Advanced Materials* 36, no. 15 (2024): 2311009.

142. Y. Shang, N. Chen, Y. Li, et al., "An "Ether-in-Water" Electrolyte Boosts Stable Interfacial Chemistry for Aqueous Lithium-Ion Batteries," *Advanced Materials* 32, no. 40 (2020): 2004017.

143. T. Zhou, Y. Mu, L. Chen, et al., "Toward Stable Zinc Aqueous Rechargeable Batteries by Anode Morphology Modulation via Poly-aspartic Acid Additive," *Energy Storage Materials* 45 (2022): 777–785.

144. Y. Wang, Y. Zhao, S. Zhang, et al., "Monofluorinated Phosphate With Unique P-F Bond for Nonflammable and Long-Life Lithium-Ion Batteries," *Angewandte Chemie International Edition* 63 (2024): e202412108.

145. S. Li, X. Shen, B. Zhao, et al., "An Improved N–N Dimethylacetamide-Based Non-Flammable Molecular Crowding Electrolyte Using NaOTf for Cobalt-Based Prussian Blue//Hard Carbon Aqueous Solution Battery," *Journal of Colloid and Interface Science* 678 (2025): 732–740.

146. L. Cao, D. Li, E. Hu, et al., "Solvation Structure Design for Aqueous Zn Metal Batteries," *Journal of the American Chemical Society* 142, no. 51 (2020): 21404–21409.

147. Q. Nian, J. Wang, S. Liu, et al., "Aqueous Batteries Operated at −50°C," *Angewandte Chemie* 131, no. 47 (2019): 17150–17155.

148. W. Yang, X. Du, J. Zhao, et al., "Hydrated Eutectic Electrolytes With Ligand-Oriented Solvation Shells for Long-Cycling Zinc-Organic Batteries," *Joule* 4, no. 7 (2020): 1557–1574.

149. Y. Ma, Q. Zhang, L. Liu, et al., "*N*,*N*-Dimethylformamide Tailors Solvent Effect to Boost Zn Anode Reversibility in Aqueous Electrolyte," *National Science Review* 9, no. 10 (2022): nwac051.

150. X. Zhou, Y. Lu, Q. Zhang, et al., "Exploring the Interfacial Chemistry Between Zinc Anodes and Aqueous Electrolytes via an In Situ Visualized Characterization System," *ACS Applied Materials & Interfaces* 12, no. 49 (2020): 55476–55482.

151. P. Jaumaux, X. Yang, B. Zhang, et al., "Localized Water-In-Salt Electrolyte for Aqueous Lithium-Ion Batteries," *Angewandte Chemie International Edition* 60, no. 36 (2021): 19965–19973.

152. S. Mehta, S. Kaur, M. Singh, et al., "Unleashing Ultrahigh Capacity and Lasting Stability: Aqueous Zinc-Sulfur Batteries," *Advanced Energy Materials* 14, no. 27 (2024): 2401515.

153. D. Patel, A. Dharmesh, Y. Sharma, P. Rani, and A. K. Sharma, "Hybrid Electrolyte With Biomass-Derived Carbon Host for High-Performance Aqueous Zn–S Battery," *Chemical Engineering Journal* 479 (2024): 147722.

154. T. S. Thomas, A. P. Sinha, and D. Mandal, "Modulating Electrolyte Solvation for High-Performance Aqueous Zinc–Sulfur Batteries," *Journal of Materials Chemistry A* 12, no. 32 (2024): 21350–21356.

155. Y. Li, X. Zheng, E. Z. Carlson, et al., "In Situ Formation of Liquid Crystal Interphase in Electrolytes With Soft Templating Effects for Aqueous Dual-Electrode-Free Batteries," *Nature Energy* 9, no. 11 (2024): 1350–1359.

156. B. Liu, J. Ma, J. Feng, T. Lin, and L. Suo, "Bifunctional Fluorocarbon Electrode Additive Lowers the Salt Dependence of Aqueous Electrolytes," *Advanced Materials* 36 (2024): 2413573.

157. X. Yu, M. Chen, J. Wang, et al., "Deciphering Multi-Dimensional Interfacial Mechanisms via Organic Cosolvent Engineering for Sustainable Zinc Metal Batteries," *Nature Communications* 16, no. 1 (2025): 3820.

158. Y. Tang, J. H. Li, C. L. Xu, M. Liu, B. Xiao, and P. F. Wang, "Electrode/Electrolyte Interfacial Engineering for Aqueous Zn-Ion Batteries," *Carbon Neutralization* 2, no. 2 (2023): 186–212.

159. X. Fu, R. Shi, Y. Liu, et al., "Expanding the Temperature Range of Stable Aqueous Batteries: Strategies, Mechanisms and Perspectives," *Energy & Environmental Science* 18, no. 5 (2025): 2165–2215.

160. X. Yang, J. Zhou, B. Hao, et al., "Tailoring Cold-Resilient Electrolytes Driven by Mechanisms Underlying Ice Melting for Cryogenic Zn Batteries," *Advanced Materials* (2025): 2506537.

161. L. He, C. Lin, P. Xiong, et al., "Progress in Electrolyte Engineering of Aqueous Batteries in a Wide Temperature Range," *Transactions of Tianjin University* 29, no. 5 (2023): 321–346.

162. L. Suo, D. Oh, Y. Lin, et al., "How Solid-Electrolyte Interphase Forms in Aqueous Electrolytes," *Journal of the American Chemical Society* 139, no. 51 (2017): 18670–18680.

163. Z. Tong, T. Kang, Y. Wan, et al., "A Ca-Ion Electrochromic Battery via a Water-in-Salt Electrolyte," *Advanced Functional Materials* 31, no. 41 (2021): 2104639.

164. Y. Wang, W. Pan, K. W. Leong, et al., "Paper-Based Aqueous Al Ion Battery With Water-in-Salt Electrolyte," *Green Energy & Environment* 8, no. 5 (2023): 1380–1388.

165. P. K. Jha, S. Kochrekar, A. Jadhav, et al., "Wide Electrochemical Stability Window of $NaClO_4$ Water-in-Salt Electrolyte Elevates the Supercapacitive Performance of Poly(3,4-Ethylenedioxythiophene)," *Energy Storage Materials* 72 (2024): 103758.

166. Z. Guo, Y. Zhao, Y. Ding, et al., "Multi-Functional Flexible Aqueous Sodium-Ion Batteries With High Safety," *Chem* 3, no. 2 (2017): 348–362.

167. T. Sun, X. Yuan, K. Wang, et al., "An Ultralow-Temperature Aqueous Zinc-Ion Battery," *Journal of Materials Chemistry A* 9, no. 11 (2021): 7042–7047.

168. L. Jiang, X. Luo, and D. W. Wang, "A Review on System and Materials for Aqueous Flexible Metal–Air Batteries," *Carbon Energy* 5, no. 3 (2023): e284.

169. W. Wang, C. Li, S. Liu, et al., "Flexible Quasi-Solid-State Aqueous Zinc-Ion Batteries: Design Principles, Functionalization Strategies, and Applications," *Advanced Energy Materials* 13, no. 18 (2023): 2300250.

170. M. Al-Abbasi, Y. Zhao, H. He, et al., "Challenges and Protective Strategies on Zinc Anode Toward Practical Aqueous Zinc-Ion Batteries," *Carbon Neutralization* 3, no. 1 (2024): 108–141.

171. H. Li, J. Hao, and S. Z. Qiao, "AI-Driven Electrolyte Additive Selection to Boost Aqueous Zn-Ion Batteries Stability," *Advanced Materials* 36, no. 49 (2024): 2411991.

172. Y. C. Gao, Y. H. Yuan, S. Huang, et al., "Frontispiece: A Knowledge–Data Dual-Driven Framework for Predicting the Molecular Properties of Rechargeable Battery Electrolytes," *Angewandte Chemie International Edition* 64, no. 4 (2025): e202416506.

Supporting Information

Additional supporting information can be found online in the Supporting Information section.

Revised Supporting Information. **Table S1:** Comparison Table of Metal Characteristics and Energy - Storage Performance of Different Metal Batteries. **Table S2:** The change of ESW of different aqueous electrolytes. **Table S3:** Cost estimation data for different systems. **Figure S1:** Schematic of discharge process on α-MnO_2 cathode, where ion-pairs offset (or do not contribute to) the ionic current and the slow Zn^{2+} intercalation process is suppressed by fast H^+ intercalation. Reproduced with permission: Copyright 2023, Mater. Today [30]. **Figure S2:** The corresponding crystal structure of N-NaVTP. Reproduced with permission: Copyright 2024, Small [55]. **Figure S3:** Coulombic efficiency and cycling performance of Zn metals in Cu || Zn cells under current density of 1 mA cm^{-2} for 1 mAh cm^{-2}. Reproduced with permission: Copyright 2020, Adv. Funct. Mater [66]. **Figure S4:** H^+/OH^- ionization mechanism and electrolyte structure of the aqueous $AlAc(OH)_2$ electrolyte. Reproduced with permission: Copyright 2024, J. Am. Chem. Soc [82]. **Figure S5:** Low and high (inset) magnification SEM images of HiSE. Reproduced with permission: Copyright 2022, Energy Storage Mater [87]. **Figure S6:** Molecular dynamics (MD) simulations of the Al^{3+}-solvation structure in Supporting Figure 5A-D. A: A snapshot of the MD simulation for WISE (2 M $Al(OTf)_3$+20 M LiTFSI electrolyte) at 390 K; B: Representative Al^{3+}-solvation structures in electrolytes with 2 M $Al(OTf)_3$ and three LiTFSI concentrations (5 M, 10 M and 20 M) ; C: Al^{3+}-O ($TFSI^-$ /OTf^-) and D: Al^{3+}-O (water) coordination numbers for electrolytes with 2 M $Al(OTf)_3$ and three LiTFSI concentrations (5 M, 10 M and 20 M). Reproduced with permission: Copyright 2024, Green Energy Environ [96]. **Figure S7:** Galvanostatic Zn plating/stripping in the Zn || Zn symmetrical cell at 0.5 mA cm^{-2} and 0.5 mAh cm^{-2}. Reproduced with permission: Copyright 2021, Angew. Chem. Int. Ed [100]. **Figure S8:** MD simulated pair distribution function and coordination numbers of Na with O-atom from water (Ow), ClO_4 (OCl), and OTF (OOTF) in the 17 M $NaClO_4$ and 19 M $NaClO_4$–NaOTF. Reproduced with permission: Copyright 2021, Angew. Chem. Int. Ed [101]. **Figure S9:** High-energy aqueous Li-ion batteries. Cycling stability and Coulombic efficiency of $LiMn_2O_4$ || passivated-$Li_4Ti_5O_{12}$ full cell with the 63 M WIHS aqueous gel electrolyte (42 M LiTFSI + 21 M Pyr_{14}·TFSI) at the rate of 0.2 C. Reproduced with permission: Copyright 2020, ACS Energy Lett [103]. **Figure S10:** Zn^{2+}-conducting SEI, characterized by small nodular particles embedded in a polymeric framework. Reproduced with permission: Copyright 2021, Nat. Nanotechnol ACS Energy Lett [105]. **Figure S11:** A Novel "Water-in-Ionic Liquid" Electrolyte for Zn Metal Batteries. Reproduced with permission: Copyright 2023, Nat. Nanotechnol ACS Energy Lett [109]. **Figure S12:** The schematic description of the role of multivalence ion in the formation of anion-derived SEI on Li metal anode surface in the designed BE MgLN electrolyte. Reproduced with permission: Copyright 2022, Angew. Chem. Int. Ed [122]. **Figure S13:** Electrochemical performances of the $Na_{0.44}MnO_2$ plates in different electrolytes. Long term cycling performances of NMOs at 100 mA g^{-1}. Reproduced with permission: Copyright 2020, ACS Appl. Mater. Interfaces [130]. **Figure S14:** Stripping/plating performance of Zn || Zn symmetrical battery. Reproduced with permission: Copyright 2020, ACS Appl. Mater. Interfaces [149]. **Figure S15:** Long-term cycling of PDB in ZW (0.15 C) and ZS (0.15 and 0.30 C) respectively. Reproduced with permission: Copyright 2020, Joule [150]. **Figure S16:** Comparison of our work with reported zinc-ion and zinc-sulfur batteries performance. Reproduced with permission: Copyright 2024, Adv. Energy Mater [151]. **Figure S17:** Cost - estimation of different rechargeable battery electrolyte systems. The data, sourced from commodities, was collected through systematic research with the deadline set as June 2025[12,119,147,154].

Optimization Strategies and Mechanisms of High-Concentration Electrolytes for Aqueous Rechargeable Batteries

Lingli Chen[1], Yue Xu[1,2,3*], Angran Liu[1], Bo Cheng[1], Sihan Wang[1], Xiaolin Zhang[3], Yongbin Hua[1], Long Jiang[1], Chun Fang[2*], Jiantao Han[2], and Paul K. Chu[3]

[1]School of Physic and Optoelectronic Engineering, Yangtze University, Jingzhou 434023, China

[2] School of Materials Science and Engineering and State Key Laboratory for Materials Processing and Die & Mould Technology, Huazhong University of Science and Technology, Wuhan 430074, China

[3] Department of Physics, City University of Hong Kong, Tat Chee Avenue, Kowloon, Hong Kong, China

[*]Correspondence: Prof. Yue Xu (yuexu@yangtzeu.edu.cn), Prof. Chun Fang (fangchun@hust.edu.cn)

Table S1. Comparison Table of Metal Characteristics and Energy - Storage Performance of Different Metal Batteries

Metals	**Abundance [ppm]**	**Reduction potential [V]**	**Ionic radii [Å]**	**Hydrated radii [Å]**	**Specific capacity [mAh g^{-1}]**	**Volumetric energy [mAh mL^{-1}]**
Li	18	-3.04	0.6	3.82	3862	2061
Na	22700	-2.71	0.95	3.58	1166	1129
K	15000	-2.93	1.33	3.31	685	610
Ca	46600	-2.87	0.99	4.12	1337	2072
Mg	27640	-2.37	0.65	4.28	2205	3834
Zn	79	-0.76	0.74	4.3	820	5851
Al	83000	-1.66	0.5	4.75	2980	8046

Comparison of abundance, redox potentials, ionic, and hydrated radius along with charge storage capacities of various metal batteries. Reproduced with permission: Copyright 2023, Adv. Mater[49].

Table S2. The change of ESW of different aqueous electrolytes.

Electrolyte	ESW	CE(%)	Time	Refs.
1M NaNO3 + 1M LiNO3	1.5V(-0.5~1)	~100%	2018	[83]
7 m LiOTf + 21 m LiTFSI	1.83~4.9V	97%	2016	[89]
42 m LiTFSI + 21 m Me_3EtN·TFSI	3.25V(1.75~5.0V)	95%	2020	[103]
17 m $NaClO_4$ + 2 m NaOTF	2.8V(1.6~4.4V)	99.8%	2021	[107]
$LiNO_3·3H_2O$+$NaNO_3$	3.1V(2.15~5.23V)	-	2021	[123]
NaOTf+PC	2.8V(-1.25~1.55V)	99.8%	2018	[135]
21 m LiTFSI + 7 m LiOTf	4.1V(1~5.1V)	~100%	2018	[136]
LiTFSI+TEGDME	4.2V(0.6V~4.8V)	99.66%	2020	[137]
LiTFSI+IDE	4.3V(0.8~5.1V)	99.68%	2024	[144]

The ESW ranges and coulombic efficiencies of different electrolytes published in different periods are compared [83,89,103,107,123,135–137,144].

Table S3. Cost estimation data for different systems.

Systems	Composition	Price	Index
Normal	2 M $LiPF_6$ + DMC	$LiPF_6$ ≈ \$7.23/kg, DMC ≈ \$1/kg	100
WISE	21 M LiTFSI	LiTFSI ≈ \$75/kg	3597
Fluorine-free WIBS	32 M KOAc + 8 M LiAc	KOAc ≈ \$1.25/kg, LiAc ≈ \$20/kg	173
Co-solvents	2M $NaClO_4$ + 0.3M DMSO	$NaClO_4$≈ \$1.6/kg, DMSO≈ \$2.5/kg	24
LCE	12.5 M $LiNO_3$ + H_2O : PD = 1:1	$LiNO_3$ ≈ \$13.9/kg, PD≈ \$5.56/kg	443

Cost - estimation of different rechargeable battery electrolyte systems. The data, sourced from commodities, was collected through systematic research with the deadline set as June 2025[12,119,147,154].

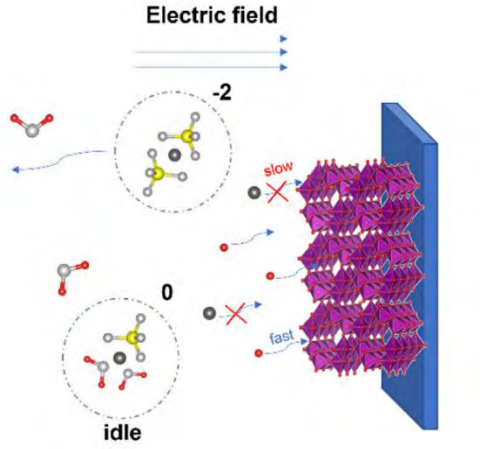

Figure S1. Schematic of discharge process on α-MnO_2 cathode, where ion-pairs offset (or do not contribute to) the ionic current and the slow Zn^{2+} intercalation process is suppressed by fast H^+ intercalation. Reproduced with permission: Copyright 2023, Mater. Today [30].

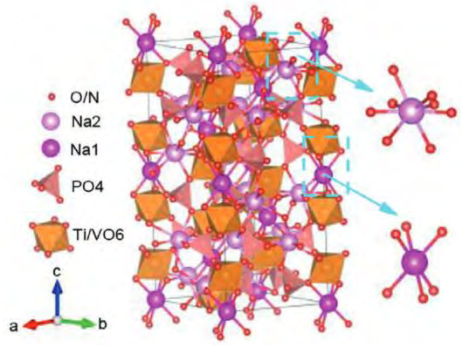

Figure S2. The corresponding crystal structure of N-NaVTP. Reproduced with permission: Copyright 2024, Small [55].

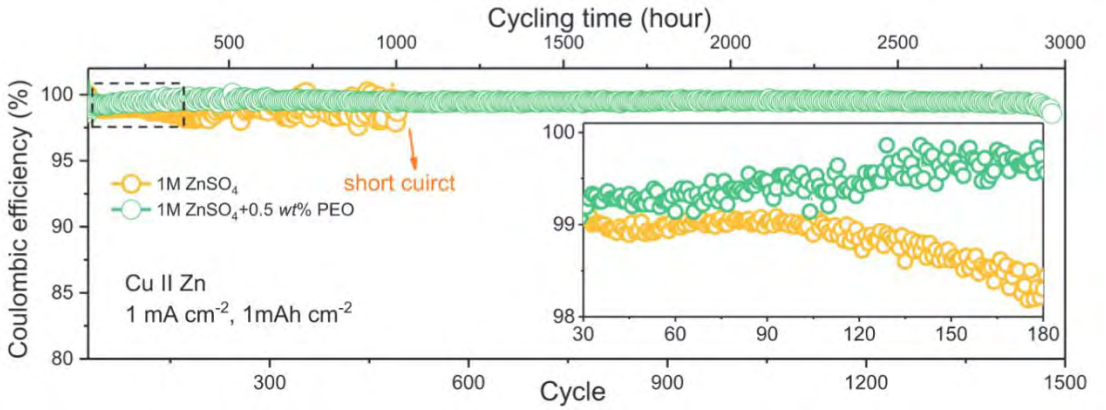

Figure S3. Coulombic efficiency and cycling performance of Zn metals in Cu || Zn cells under current density of 1 mA cm^{-2} for 1 mAh cm^{-2}. Reproduced with permission: Copyright 2020, Adv. Funct. Mater [66].

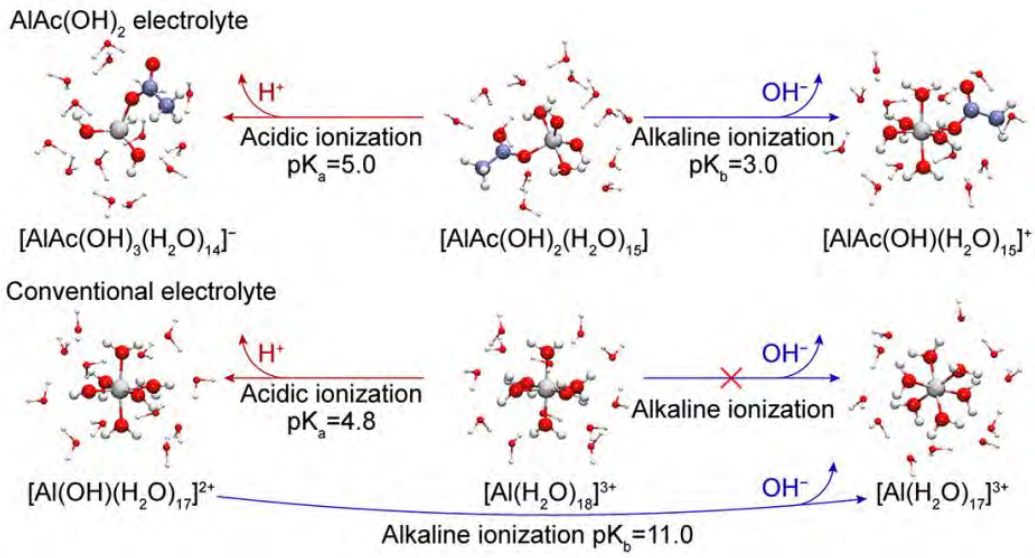

Figure S4. H^+/OH^- ionization mechanism and electrolyte structure of the aqueous $AlAc(OH)_2$ electrolyte. Reproduced with permission: Copyright 2024, J. Am. Chem. Soc [82].

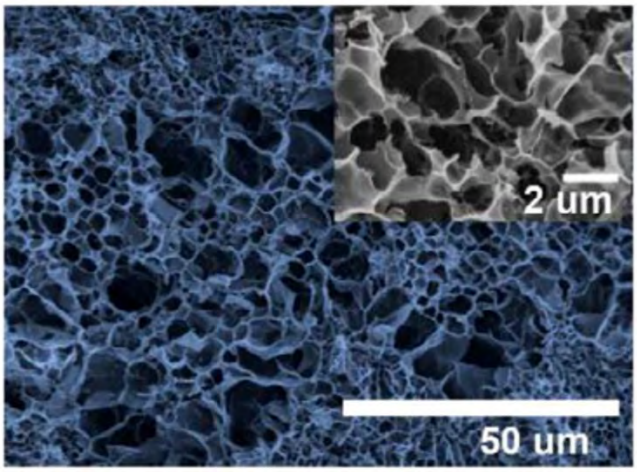

Figure S5. Low and high (inset) magnification SEM images of HiSE. Reproduced with permission: Copyright 2022, Energy Storage Mater [87].

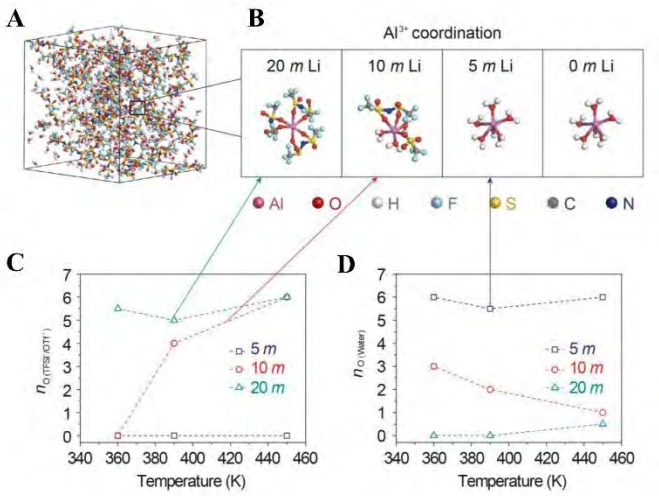

Figure S6. Molecular dynamics (MD) simulations of the Al^{3+}-solvation structure in Supplementary Figure 5A-D. A: A snapshot of the MD simulation for WISE (2 M $Al(OTf)_3$+20 M LiTFSI electrolyte) at 390 K; B: Representative Al^{3+}-solvation structures in electrolytes with 2 M $Al(OTf)_3$ and three LiTFSI concentrations (5 M, 10 M and 20 M)； C: Al^{3+}-O ($TFSI^-$ /OTf^-) and D: Al^{3+}-O (water) coordination numbers for electrolytes with 2 M $Al(OTf)_3$ and three LiTFSI concentrations (5 M, 10 M and 20 M). Reproduced with permission: Copyright 2024, Green Energy Environ [96].

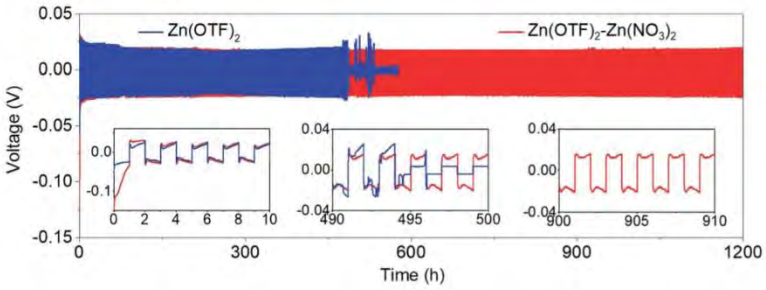

Figure S7. Galvanostatic Zn plating/stripping in the Zn || Zn symmetrical cell at 0.5 mA cm^{-2} and 0.5 mAh cm^{-2}. Reproduced with permission: Copyright 2021, Angew. Chem. Int. Ed [100].

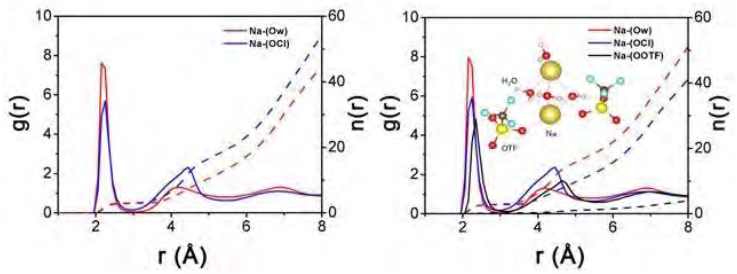

Figure S8. MD simulated pair distribution function and coordination numbers of Na with O-atom from water (Ow), ClO_4 (OCl), and OTF (OOTF) in the 17 M $NaClO_4$ and 19 M $NaClO_4$–NaOTF. Reproduced with permission: Copyright 2021, Angew. Chem. Int. Ed [101].

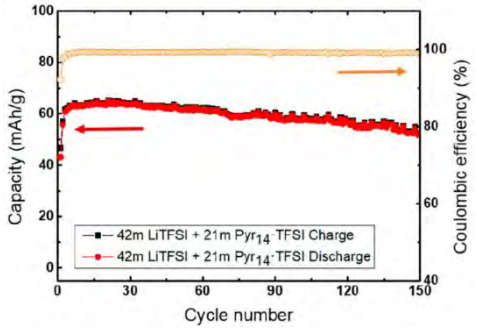

Figure S9. High-energy aqueous Li-ion batteries. Cycling stability and Coulombic efficiency of $LiMn_2O_4$ || passivated-$Li_4Ti_5O_{12}$ full cell with the 63 M WIHS aqueous gel electrolyte (42 M LiTFSI + 21 M Pyr_{14}·TFSI) at the rate of 0.2 C. Reproduced with permission: Copyright 2020, ACS Energy Lett [103].

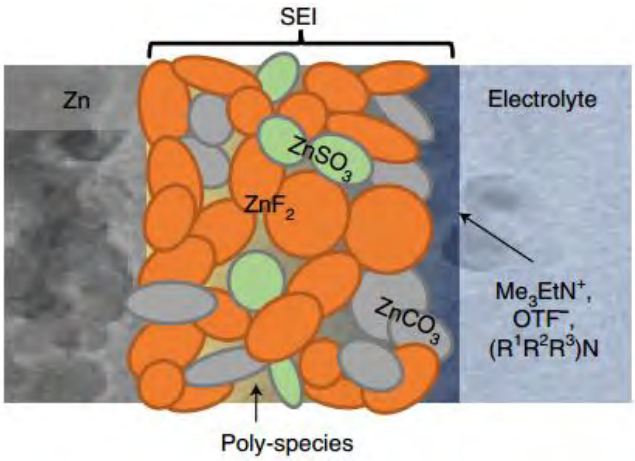

Figure S10. Zn^{2+}-conducting SEI, characterized by small nodular particles embedded in a polymeric framework. Reproduced with permission: Copyright 2021, Nat. Nanotechnol ACS Energy Lett [105].

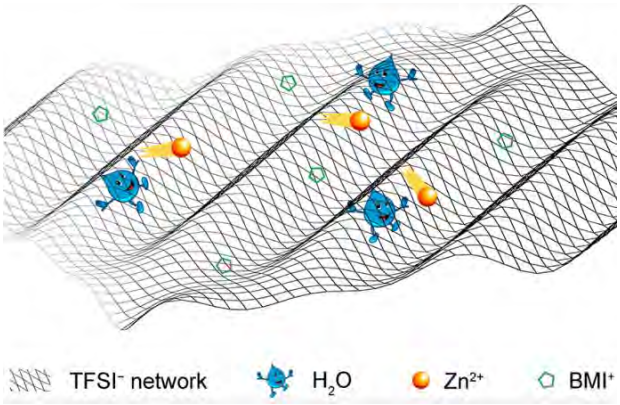

Figure S11. A Novel “Water-in-Ionic Liquid” Electrolyte for Zn Metal Batteries. Reproduced with permission: Copyright 2023, Nat. Nanotechnol ACS Energy Lett [109].

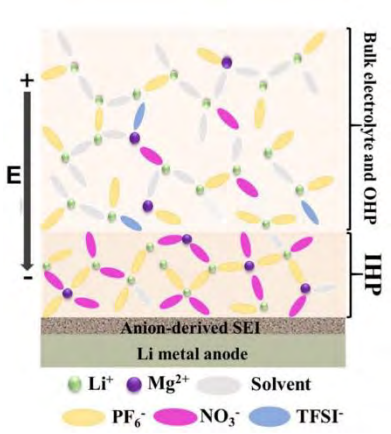

Figure S12. The schematic description of the role of multivalence ion in the formation of anion-derived SEI on Li metal anode surface in the designed BE MgLN electrolyte. Reproduced with permission: Copyright 2022, Angew. Chem. Int. Ed [122].

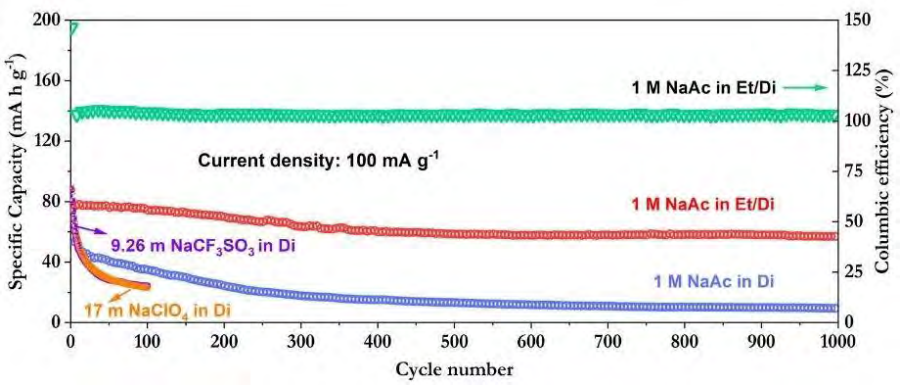

Figure S13. Electrochemical performances of the $Na_{0.44}MnO_2$ plates in different electrolytes. Long term cycling performances of NMOs at 100 mA g^{-1}. Reproduced with permission: Copyright 2020, ACS Appl. Mater. Interfaces [130].

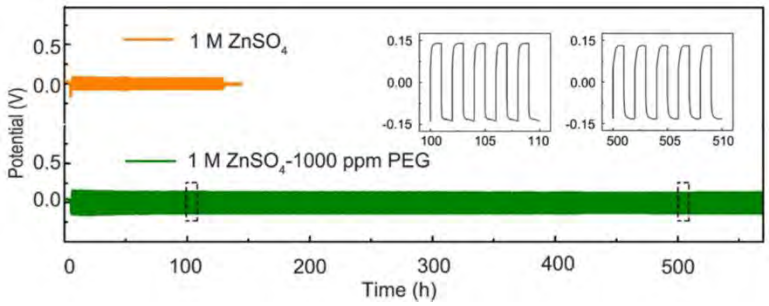

Figure S14. Stripping/plating performance of Zn || Zn symmetrical battery. Reproduced with permission: Copyright 2020, ACS Appl. Mater. Interfaces [149].

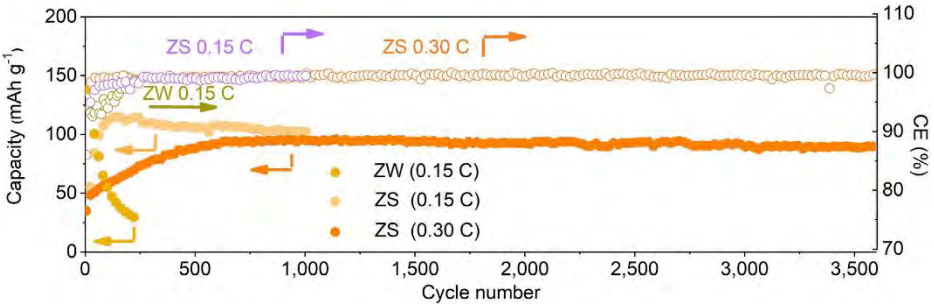

Figure S15. Long-term cycling of PDB in ZW (0.15 C) and ZS (0.15 and 0.30 C) respectively. Reproduced with permission: Copyright 2020, Joule [150].

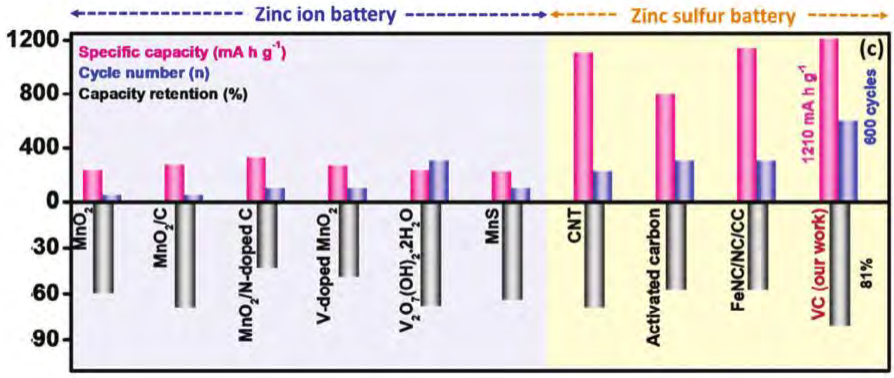

Figure S16. Comparison of our work with reported zinc-ion and zinc-sulfur batteries performance. Reproduced with permission: Copyright 2024, Adv. Energy Mater [151].

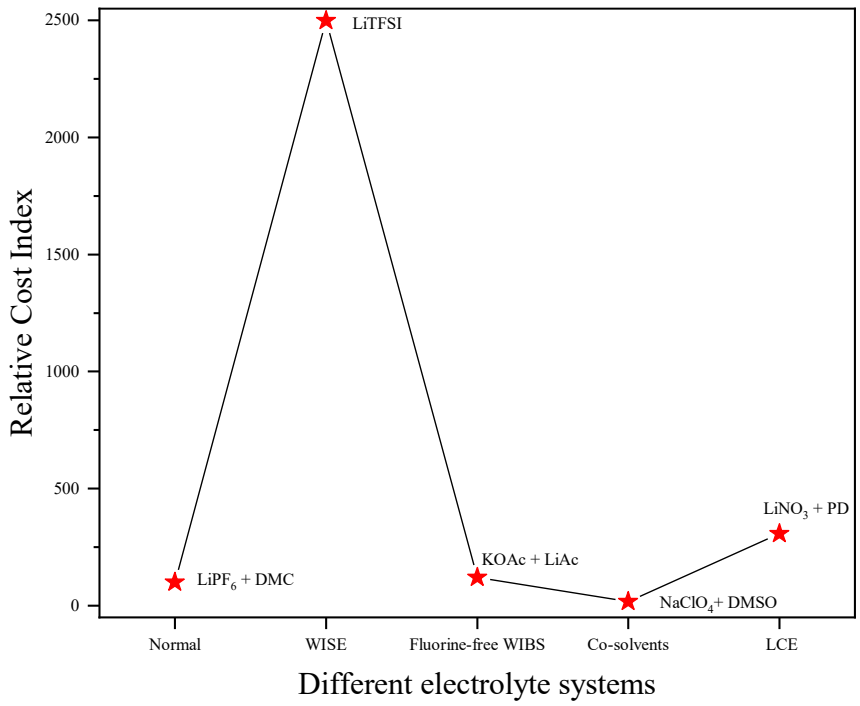

Figure S17. Cost - estimation of different rechargeable battery electrolyte systems. The data, sourced from commodities, was collected through systematic research with the deadline set as June 2025[12,119,147,154].

REFERENCES

12. L. Suo, O. Borodin, T. Gao, et al., "“Water-in-Salt” Electrolyte Enables High-Voltage Aqueous Lithium-Ion Chemistries," Science 350, no. 6263 (2015): 938–943.

30. Y. Xu, X. Zhou, Z. Chen, Y. Hou, Y. You, and J. Lu, "Electrolyte Formulas of Aqueous Zinc Ion Battery: A Physical Difference With Chemical Consequences," Materials Today 66, (2023): 339–347.

49. Z. Khan, D. Kumar, and X. Crispin, "Does Water-in-Salt Electrolyte Subdue Issues of Zn Batteries?," Advanced Materials 35, no. 36 (2023): 2300369.

55. Q. Y. Meng, J. C. Shao, X. R. Dou, and H. Z. Chi, "N-Containing Na2VTi(PO4)3/C for Aqueous Sodium-Ion Batteries," Small 20, no. 28 (2024): 2308483.

66. Y. Jin, K. S. Han, Y. Shao, et al., "Stabilizing Zinc Anode Reactions by Polyethylene Oxide Polymer in Mild Aqueous Electrolytes," Advanced Functional Materials 30, no. 43 (2020): 2003932.

82. Q. Zhang, X. Liu, Y. Lu, et al., "Sustainable Aqueous Batteries Based on Bipolar Dissociation of Aluminum Hydroxyacetate Electrolyte," Journal of the American Chemical Society 146, no. 8 (2024): 5597–5604.

83. Q. Yang, W. Wang, H. Li, J. Zhang, F. Kang, and B. Li, "Investigation of Iron Hexacyanoferrate as a High Rate Cathode for Aqueous Batteries: Sodium-Ion Batteries and Lithium-Ion Batteries," Electrochimica Acta 270, (2018): 96–103.

87. L. Sun, Y. Yao, L. Dai, et al., "Sustainable and High-Performance Zn Dual-Ion Batteries with a Hydrogel-Based Water-in-Salt Electrolyte," Energy Storage Materials 47, (2022): 187–194.

89. L. Suo, O. Borodin, W. Sun, et al., "Advanced High-Voltage Aqueous Lithium-Ion Battery Enabled by “Water-in-Bisalt” Electrolyte," Angewandte Chemie International Edition 55, no. 25 (2016): 7136–7141.

96. W. Tang, L. Deng, L. Guo, S. Zhou, Q. Jiang, and J. Luo, "Reversible Aqueous Aluminum Metal Batteries Enabled by a Water-in-Salt Electrolyte," Green Energy & Environment 9, no. 7 (2024): 1183–1191.

100. D. Li, L. Cao, T. Deng, S. Liu, and C. Wang, "Design of a Solid Electrolyte Interphase for Aqueous Zn Batteries," Angewandte Chemie International Edition 60, no. 23 (2021): 13035–13041.

101. T. Jin, X. Ji, P. Wang, et al., "High-Energy Aqueous Sodium-Ion Batteries," Angewandte Chemie International Edition 60, no. 21 (2021): 11943–11948.

103. L. Chen, J. Zhang, Q. Li, et al., "A 63 m Superconcentrated Aqueous Electrolyte for High-Energy Li-Ion Batteries," ACS Energy Letters 5, no. 3 (2020): 968–974.

105. L. Cao, D. Li, T. Pollard, et al., "Fluorinated Interphase Enables Reversible Aqueous Zinc Battery Chemistries," Nature Nanotechnology 16, no. 8 (2021): 902–910.

109. Z. Zhao, J. Lai, D. T. Ho, et al., "A Novel “Water-in-Ionic Liquid” Electrolyte for Zn Metal Batteries," ACS Energy Letters 8, no. 1 (2023): 608–618.

119. W. Deng, X. Wang, C. Liu, et al., "Li/K Mixed Superconcentrated Aqueous Electrolyte Enables

High-Performance Hybrid Aqueous Supercapacitors," Energy Storage Materials 20, (2019): 373–379.

122. S. Liu, J. Xia, W. Zhang, et al., "Salt-in-Salt Reinforced Carbonate Electrolyte for Li Metal Batteries," Angewandte Chemie International Edition 61, no. 43 (2022): e202210522.

123. Z. Wang, Y. Xu, J. Peng, et al., "A High Rate and Stable Hybrid Li/Na-Ion Battery Based on a Hydrated Molten Inorganic Salt Electrolyte," Small 17, no. 40 (2021): 2101650.

130. R. Chua, Y. Cai, P. Q. Lim, et al., "Hydrogen-Bonding Interactions in Hybrid Aqueous/Nonaqueous Electrolytes Enable Low-Cost and Long-Lifespan Sodium-Ion Storage," ACS Applied Materials & Interfaces 12, no. 20 (2020): 22862–22872.

135. H. Zhang, B. Qin, J. Han, and S. Passerini, "Aqueous/Nonaqueous Hybrid Electrolyte for Sodium-Ion Batteries," ACS Energy Letters 3, no. 7 (2018): 1769–1770.

136. F. Wang, O. Borodin, M. S. Ding, et al., "Hybrid Aqueous/Non-aqueous Electrolyte for Safe and High-Energy Li-Ion Batteries," Joule 2, no. 5 (2018): 927–937.

137. J. Zhu, Y. Xu, Y. Fu, et al., "Hybrid Aqueous/Nonaqueous Water-in-Bisalt Electrolyte Enables Safe Dual Ion Batteries," Small 16, no. 17 (2020): 1905838.

144. H. Fei, F. Yang, Z. Jusys, S. Passerini, and A. Varzi, "Ethylene Glycol Co-Solvent Enables Stable Aqueous Ammonium-Ion Batteries with Diluted Electrolyte," Advanced Functional Materials (2024): 2404560.

147. Q. Nian, J. Wang, S. Liu, et al., "Aqueous Batteries Operated at −50°C," Angewandte Chemie 131, no. 47 (2019): 17150–17155.

149. X. Zhou, Y. Lu, Q. Zhang, et al., "Exploring the Interfacial Chemistry between Zinc Anodes and Aqueous Electrolytes via an In Situ Visualized Characterization System," ACS Applied Materials & Interfaces 12, no. 49 (2020): 55476–55482.

150. W. Yang, X. Du, J. Zhao, et al., "Hydrated Eutectic Electrolytes with Ligand-Oriented Solvation Shells for Long-Cycling Zinc-Organic Batteries," Joule 4, no. 7 (2020): 1557–1574.

151. S. Mehta, S. Kaur, M. Singh, et al., "Unleashing Ultrahigh Capacity and Lasting Stability: Aqueous Zinc-Sulfur Batteries," Advanced Energy Materials 14, no. 27 (2024): 2401515.

154. P. Jaumaux, X. Yang, B. Zhang, et al., "Localized Water-In-Salt Electrolyte for Aqueous Lithium-Ion Batteries," Angewandte Chemie International Edition 60, no. 36 (2021): 19965–19973.